NASA Technical Memorandum 109082

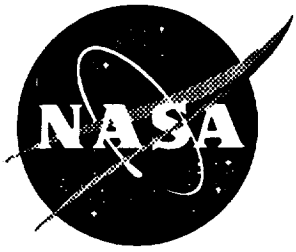

Implementation of Thermal Residual Stresses in the Analysis of Fiber Bridged Matrix Crack Growth in Titanium Matrix Composites

J. G. Bakuckas, Jr.
Galaxy Scientific Corporation, Pleasantville, New Jersey

W. S. Johnson
Langley Research Center, Hampton, Virginia

February 1994

National Aeronautics and
Space Administration
Langley Research Center
Hampton, Virginia 23681-0001

IMPLEMENTATION OF THERMAL RESIDUAL STRESSES IN THE ANALYSIS OF FIBER BRIDGED MATRIX CRACK GROWTH IN TITANIUM MATRIX COMPOSITES

J. G. BAKUCKAS, JR[1]*. AND W. S. JOHNSON*[2]
Mechanics of Materials Branch
Materials Division
NASA Langley Research Center
Hampton, Virginia 23681

Key Words: Fiber-matrix debonding, stress intensity factor, crack growth, metal matrix composites micromechanics, fracture mechanics.

ABSTRACT

In this research, thermal residual stresses were incorporated in an analysis of fiber-bridged matrix cracks in unidirectional and cross-ply titanium matrix composites (TMC) containing center holes or center notches. Two TMC were investigated, namely, SCS-6/Ti-15-3 and SCS-6/Timetal-21S laminates. Experimentally, matrix crack initiation and growth were monitored during tension-tension fatigue tests conducted at room temperature and at an elevated temperature of 200°C. Analytically, thermal residual stresses were included in a fiber bridging (FB) model. The local R-ratio and stress-intensity factor in the matrix due to thermal and mechanical loadings were calculated and used to evaluate the matrix crack growth behavior in the two materials studied. The frictional shear stress term, τ, assumed in this model was used as a curve-fitting parameter to matrix crack growth data. The scatter band in the values of τ used to fit the matrix crack growth data was significantly reduced when thermal residual stresses were included in the fiber bridging analysis. For a given material system, lay-up and temperature, a single value of τ was sufficient to analyze the crack growth data. It was revealed in this study that thermal residual stresses are an important factor overlooked in the original FB models.

---

[1] Former Resident Research Associate, National Research Council, Presently, Senior Research Engineer, Galaxy Scientific Corporation, 2500 English Creek Ave., Pleasantville, NJ 08232.

[2] Senior Research Scientist

NOMENCLATURE

a, a_o	Current crack length and unbridged initial crack length, m
AA'	Superscript referring to crack centerline
A_f, A_m	Cross sectional area of fiber and matrix, m^2
BB'	Superscript referring to end line of slip region
d	Hole diameter, m
C, n, m	Crack growth coefficient constants
E_f, E_m	Fiber and matrix modulus, MPa
E_L, E_T, G_{LT}	Composite longitudinal, transverse, and shear modulus, MPa
F_{app}	Boundary correction factor for applied stress-intensity factor
F_{par}	Correction factor for parallel cracks
G	Weight function
ΔK_{app}	Applied stress-intensity factor range, MPa$\sqrt{m}$
ΔK_m	Discrete stress-intensity factor range in matrix, MPa$\sqrt{m}$
ΔK_{Comp}	Continuum stress-intensity factor range in composite, MPa$\sqrt{m}$
ℓ	Slip length, m
ℓ_R	Slip length of frictional shear stress reversal, m
h	Distance between parallel cracks, m
max	Superscript referring to maximum applied load
min	Superscript referring to minimum applied load
Δp	Range in bridging pressure, MPa
r	Fiber radius, m
R	Hole radius, m
R_{Comp}	Composite stress ratio = S^{min}/S^{max}
R_m	Matrix stress ratio = $\sigma_m^{min}/\sigma_m^{max}$
ΔS	Applied stress range, MPa
ΔT	Change in temperature, °C
v_f, v_m	Fiber and matrix volume fractions
W	Width of specimen, m
$\tilde{x}$	Integration variable along crack from center, m
α_f, α_m	Coefficient of thermal expansion for fiber and matrix, mm/mm/°C
$\Delta\delta_{Comp}$	Continuum crack opening displacement range in composite, m
$\Delta\delta_m$	Discrete crack opening displacement range in matrix, m
γ_{Comp}	Composite fracture surface energy = K_{Comp}^2/E_L MN/m
γ_m	Matrix fracture surface energy = K_m^2/E_m MN/m
τ	Interfacial frictional shear stress, MPa
ν_{LT}	Composite Poisson's ratio

σ_f, σ_m Axial stress in fiber and matrix, MPa

σ_m^{Therm} Axial thermal residual stresses in the matrix, MPa

INTRODUCTION

In several studies [1-4], fiber-bridged matrix cracking has been identified as a major fatigue failure mechanism in titanium matrix composites (TMC). Reductions of up to 38% in the composite longitudinal stiffness and static notched strength of cross-ply SCS-6/Ti-15-3 laminates containing center holes have been reported due to fiber bridged matrix cracking [4]. Efforts to analyze the growth of these cracks using fiber bridging (FB) models have been undertaken in many investigations [5-10]. In these FB models, it is assumed that fiber-matrix debonding occurs as the matrix crack progresses past a fiber and a constant, but unknown, shear stress τ acts along the debond length. The FB models combine a continuum fracture mechanics analysis and a micromechanics analysis to obtained stress-intensity factor solutions for fiber-bridged matrix cracks.

In the research reported in [6], several of the original FB models were used to evaluate fiber-bridged matrix crack growth in unidirectional TMC. The frictional shear stress τ assumed in the FB models was used as a fitting parameter for various data sets. In this study, it was shown that the FB models are an efficient and relatively simple engineering tool to conduct parametric analyses using the composite microstructural variables and may provide the framework for a damage tolerance methodology. There are, however, several shortcomings of the FB models that were pointed out in this study.

Many aspects of fiber bridging crack growth were overlooked in the original FB models. The micromechanics analysis is based on a simplified one-dimensional force balance analysis of a single fiber in the wake of the matrix crack. Thus, these FB models do not account for the complex crack-tip singularity fields and the three-dimensional effects of crack front bowing around the fibers which can reduce the stress-intensity factor [11]. In addition, the assumption that a constant frictional shear stress acts along the fiber-matrix debond region is a simple engineering approximation. Variations in fiber-matrix debonding mechanisms were observed along the debond lengths in unidirectional TMC [6] which would yield different values in the shear stress. The interface stresses would also be affected by the wear of the debonded surfaces due to fatigue loading. Moreover, the large variation in the values of τ used to evaluate the data in [6] indicated that a fundamental mechanism may be missing in the formulation of the FB models. The value of τ required to fit various data sets depended on several factors, such as the applied stress and the crack extension length, and was not a material property [6]. Consequently, the dependency of τ on so many factors poses restrictions on using the FB models in a damage tolerance methodology.

It was postulated that if the major damage growth mechanisms and the mechanics governing damage were considered in the FB model, τ should represent a material constant. One important effect overlooked in the original formulations of the FB models is thermal residual stresses. Due to the mismatch in the mechanical and thermal properties of the constituents in TMC, thermal residual stresses are induced in the fiber and matrix during the

composite fabrication process and can effect the local and global fracture and fatigue behavior. Therefore, it is essential that thermal residual stresses be considered in the analysis of TMC.

The objective of this research was to incorporate thermal residual stresses in the analysis of fiber-bridged matrix cracks in unidirectional and cross-ply TMC containing center holes or center notches. Two TMC were investigated, namely, SCS-6/Ti-15-3 and SCS-6/Timetal-21S laminates. Experimentally, constant amplitude, tension-tension fatigue tests were conducted under load control mode at a frequency of 10 Hz at room temperature and at an elevated temperature of 200°C in order to determine the effects of thermal residual stresses on the crack growth behavior. Matrix crack initiation and growth were monitored using a high magnification closed circuit television (CCTV) system, a long focal length microscopic system with image acquisition capabilities, surface and edge replicas, optical microscopy, and scanning electron microscopy (SEM). Analytically, the matrix cracking observed in the two material systems was modeled using a fiber bridging (FB) model which was modified to include the effects of thermal residual stresses. The frictional shear stress term τ assumed in this model was used as a curve fitting parameter to correlate matrix crack growth data. Experimental results were interpreted from the analysis made using the FB model.

EXPERIMENTAL PROCEDURES

Materials and Specimens

Two TMC systems were studied in this research, namely, SCS-6/Ti-15-3 and SCS-6/Timetal-21S laminates. Both material systems were fabricated by Textron by hot isostatic pressing (HIPing) titanium foils between unidirectional tapes of silicon-carbide (SCS-6) fibers having a diameter of 0.14 mm. In the SCS-6/Ti-15-3 and SCS-6/Timetal-21S laminates, fibers were held in place with molybdenum and titanium-niobium cross weave wires, respectively. The composition of matrix materials used in the SCS-6/Ti-15-3 and SCS-6/Timetal-21S laminates, were Ti-15V-3Cr-3Al-3Sn and Ti-15Mo-3Al-2.7Nb-0.2Si, respectively. For the SCS-6/Ti-15-3 laminates, the lay-ups studied were $[0]_8$ and $[0/90]_s$ with a range of measured fiber volume fractions v_f from 0.33 to 0.36. For the SCS-6/Timetal-21S laminates, the lay-ups studied were $[0/90]_s$ and $[0/90]_{2s}$ with a range of measured fiber volume fractions v_f from 0.36 to 0.38. The material properties are listed in Table 1. Notice that some of the composite laminate properties were calculated using the VISCOPLY program developed by Bahei-El-Din [13].

Specimens were machined using a diamond wheel saw into straight-sided coupons with the 0° fibers in the loading direction. Each specimen was 152.5-mm in length. Center holes having diameters (d) of 6.3±0.3-mm were drilled ultrasonically in specimens having a width of 19.1-mm. Center slits having lengths ($2a$) of 5.08-mm, 7.62-mm and 8.89-mm were machined via electo-discharged machining (EDM) in specimens having a width of 25.4-mm. The SCS-6/Ti-15-3 specimens were tested in the as-received condition while the SCS-6/Timetal-21S specimens were heat treated at a temperature of 620°C for 8 hours in a vacuum and then furnaced cooled prior to testing. To enhance optical observations and surface

replication, the surface of each specimen was polished to obtain a flat and lustrous finish. Thin sheet aluminum end tabs having dimensions 19.1-mm × 19.1-mm were bonded on the ends of all specimens in order to prevent grip failure. Information on the specimens tested is listed in Table 2.

Test Procedures

Tension-tension fatigue tests were conducted under load control with $R_{Comp} = 0.1$ (S^{min}/S^{max}) at a frequency of 10 Hz using a closed-loop servo-hydraulic test machine equipped with hydraulic grips. Most of the test results discussed in this research were generated in previous studies [6,7]. In this study, one fatigue test was conducted at room or ambient temperature and another at an elevated temperature of 200°C using a quartz-lamp heater. Matrix crack initiation and progression were monitored and recorded in real time using a closed-circuit television system (CCTV) and a long focal length microscopic system capable of magnifications up to 325×. Testing was periodically interrupted when increments in crack extension were observed to take surface replicas and to examine the specimens surface near the damaged region using a scanning electron microscope (SEM) and an optical microscope.

Analytical Procedures

Fiber bridged matrix crack growth was analyzed using the approach outlined in Figure 1. As shown, crack growth behavior is evaluated according to a version of the power law function introduced by Walker [12] which includes R-ratio effects:

$$\frac{da}{dN} = C \cdot \left(\frac{\Delta K_m}{(1 - R_m)^{(1-m)}} \right)^n \qquad (1)$$

where C, n, and m are material constants for the neat matrix material, R_m is the local stress ratio in the matrix ($R_m = \sigma_m^{min}/\sigma_m^{max}$) and ΔK_m is the Mode I stress intensity factor range in the matrix. Thermal residual stresses can be included in the analysis through the quantities R_m and ΔK_m in Equation (1).

First the stress ratio R_m is calculated. Next, an iterative procedure is used to solve for ΔK_m with a FB model. In this procedure, a value of the frictional shear stress τ is assumed. Equation (1) is then integrated numerically using Simpson's rule to obtain the crack length as a function of the number of fatigue cycles and compared with experiments. If the calculations and the experimental values do not agree, ΔK_m is recalculated using another value of τ. This iteration is continued until a value of τ is found so that ΔK_m yields an acceptable comparison

between experiments and calculations. Details of the calculation of R_m and ΔK_m are provided next.

Calculation of R_m

The stress ratio in the matrix ($R_m = \sigma_m^{min} / \sigma_m^{max}$) was calculated using the VISCOPLY code [13], a micromechanics based model. The VISCOPLY code combines the vanishing fiber diameter (VFD) model, a thermo-viscoplastic theory, and laminated plate theory to evaluate the rate-dependent, high temperature response of symmetric laminates. Using the VISCOPLY code, the average local stresses and strains in the constituents can be calculated and the global composite response can be predicted under complex thermomechanical conditions including the composite fabrication process. A more detailed description of the VISCOPLY code is provided in [13].

The thermo-viscoplastic properties of the constituents used in the calculation of R_m are reported in [13] for SCS-6/Ti-15-3 laminates and in [14] for SCS-6/Timetal-21S laminates. In order to include thermal residual stresses in the calculations, the composite fabrication process was analytically simulated by modeling the cooling down from an assumed stress-free temperature to room temperature A stress-free temperature of 555°C was used for the SCS-6/Ti-15-3 laminates and 620°C was used for the SCS-6/Timetal-21S laminates. For SCS-6/Ti-15-3 laminates, it was assumed that the stress-free condition occurs at one half the melting temperature of the titanium matrix, that is, at 555°C. For the SCS-6/Timetal-21S laminates, it was assumed that the residual stresses were removed during the heat treatment cycle at a temperature of 620°C. Values of the thermal residual stresses in the matrix in the 0° plies induced during cool-down of the composite fabrication σ_m^{Therm} are listed in Table 1.

After the cool-down, a global mechanical load cycle from S^{min} to S^{max} was applied, and the corresponding stresses in the matrix in the 0° plies were calculated. Using these values of stress, the value of R_m in the matrix in the 0° plies was calculated. Values of R_m are listed in Table 2 for each specimen tested. As revealed by the results in Table 2, the values of R_m were considerably higher than the value of the applied R-ratio ($R_{Comp} = 0.1$). Thus, the value of R_{Comp} does not represent the actual stress ratio in the matrix and the constituent R_m values listed in Table 2 should be used in the analysis.

Calculation of ΔK_m

This section describes how the stress intensity factor range in the matrix ΔK_m was calculated using a FB model which includes thermal residual stresses. As illustrated in Figure 2, it is assumed in the FB model that fiber-matrix debonding takes place as a matrix crack progresses past the fibers. The intact fibers in the wake of the matrix crack are idealized as a crack bridging pressure, Δp. An unknown but constant frictional shear stress τ is assumed to act

along the debond length of the bridging fibers. A continuum fracture mechanics analysis and a micromechanical analysis are combined using discrete-continuum relations to obtain stress intensity factor solutions for fiber bridging matrix cracks of arbitrary size.

Figure 3 is a flowchart showing the procedure used to calculate ΔK_m using a micromechanics analysis and a continuum fracture mechanics analysis. The crack opening displacement in terms of the bridging pressure obtained from both analyses are combined to yield a single non-linear integral equation in terms of the bridging pressure. Once the bridging pressure is known, ΔK_m can be determined.

Micromechanics Analysis

As described in Appendix A, the crack opening displacement of the matrix, $\Delta\delta_m$, can be expressed in terms the bridging pressure, Δp as:

$$\Delta\delta_m = \lambda \Delta p^2 \tag{2}$$

where:

$$\lambda = \frac{rE_m v_m}{4\tau v_f^2 E_f (E_f v_f + E_m v_m)} \tag{3}$$

The terms in this equation are the composite microstructural parameters as defined previously in the nomenclature list. The frictional shear stress term, τ, in Equation (3) is a difficult quantity to directly measure and was therefore used in this study as a fitting parameter to crack growth data.

Thermal residual stresses do not effect the range relationship between the crack opening displacement and the bridging pressure given by Equation (2). Thermal residual stresses, however, do effect the relationship at the maximum and minimum loads:

$$\delta_m^{max} = 2\lambda\left(p^{max}\right)^2 + 4\lambda p^{max} v_f E_f \Delta T\left(\alpha_f - \alpha_m\right) \tag{4}$$

$$\delta_m^{min} = \delta_m^{max} - \lambda\left(p^{max} - p^{min}\right)^2 \tag{5}$$

The second term in Equation (4) is the crack opening displacement due to a temperature change, ΔT, where α_f and α_m are the coefficients of thermal expansion for the fiber and matrix, respectively. Equations (4) and (5) indicate that, when $\alpha_f < \alpha_m$, the absolute crack opening displacements will increase when thermal cool-down is accounted for.

Continuum Analysis

The crack opening displacement in the composite, $\Delta\delta_{Comp}$, is:

$$\Delta\delta_{Comp} = \frac{2}{E'}\int_{x}^{a} \Delta K_{Comp} G(x,\tilde{a},R,W)d\tilde{a} \tag{6}$$

where E' is an orthotropic material constant given by the laminate properties [15]:

$$\frac{1}{E'} = \frac{1}{2E_L}\sqrt{2\left(\sqrt{\frac{E_L}{E_T}} - \nu_{LT}\right) + \frac{E_L}{G_{LT}}} \tag{7}$$

and ΔK_{Comp} is the continuum stress-intensity factor range in the composite in terms of the unknown bridging pressure Δp:

$$\Delta K_{Comp} = \Delta S\sqrt{\pi a}F_{app} - 2\int_{a_o}^{a} \Delta p G(x,a,R,W)dx \tag{8}$$

In this equation, ΔS is the applied far-field stress, F_{app} is the applied stress boundary correction factor, a_o is the initial unbridged crack length (hole radius or notch length). In addition, the term $G(x,a,R,W)$ in Equations (6) and (8) is the weight function for the bridging stress-intensity factor range. Compendiums of boundary correction factors and weight functions, F_{app} and $G(x,a,R,W)$, are provided in [16-18] for a variety of cracked specimen configurations. For the two cases studied in this research, namely symmetric cracks emanating from a center notch or a center hole, expressions for F_{app} and $G(x,a,R,W)$ are provided in Appendix B. It should be pointed out that the boundary correction factors and the weight functions in [16-18] were derived for isotropic materials and it was assumed that these terms can be applied to the orthotropic materials studied in this research

Discrete-Continuum Relations

The micromechanics and continuum analyses are combined using the relations:

$$\Delta\delta_m = f\left(\Delta\delta_{Comp}\right) \tag{9}$$

$$\Delta K_m = f\left(\Delta K_{Comp}\right) \tag{10}$$

The functions $f(\Delta\delta_{Comp})$ and $f(\Delta K_{Comp})$ are the discrete-continuum relations. The three most commonly used discrete-continuum relations were used in this study and are referred to as the Marshall, Cox and Evans (MCE) relation [8], the McCartney (MC) relation [9], and the McMeekings and Evans (ME) relation [10]. All three relations are reviewed in Appendix C. The crack opening displacements from the micromechanics analysis, Equation (2), and from the continuum analysis, Equation (6), are combined using discrete-continuum relations, Equation (9), to yield a single nonlinear integral equation in terms of the unknown bridging pressure Δp and the unknown frictional shear stress τ. For example, using the ME relation [10], $\Delta\delta_m = \Delta\delta_{Comp}$, the bridging pressure can be expressed as:

$$\Delta p^2 = \frac{2}{\lambda E'} \int_x^a \left(\Delta S \sqrt{\pi a} F_{app} - 2 \int_{a_o}^a \Delta p G(x,a,R,W)dx \right) G(x,\tilde{a},R,W)d\tilde{a} \qquad (11)$$

Assuming a value for τ, the bridging pressure Δp is solved using a Newton-Raphson iterative procedure and a Simpson-type algorithm for numerical integration. Once the bridging pressure is known, the matrix stress-intensity factor range ΔK_m can be obtained using Equations (8) and (10). Using the ME relation [10], $\Delta K_m = \Delta K_{Comp}$, the matrix stress-intensity factor becomes:

$$\Delta K_m = \Delta S \sqrt{\pi a} F_{app} - 2 \int_{a_o}^a \Delta p G(x,a,R,W)dx \qquad (12)$$

Appendix C outlines the derivation of ΔK_m using the other two discrete-continuum relations.

Application of FB Model to Cross Ply Laminates

To apply the FB model to cross-ply laminates, it was assumed the fibers in the 90° plies had no effect on the growth of fiber bridged matrix cracks. In the micromechanics analysis, the fibers in the 90° plies were assumed to have no effect on the crack growth. The 90° plies were therefore modelled as matrix material alone. This implies that the fiber volume fraction for the cross plie laminates become a half of the actual value. Therefore the values of v_f and v_m in Equation (3) were adjusted accordingly. It was also assumed that the fiber-bridged matrix cracks did not influence the far-field properties. Thus, in the continuum analysis, the actual fiber volume fraction was used in calculating the laminate properties for the orthotropic correction factor E' in Equation (7). It should be pointed out that fiber-matrix debonding has been observed in the 90° plies in cross-ply TMC resulting in a reduced composite modulus [4]. This phenomena, however, was not accounted for in this research.

Modeling Parallel Cracks

Crack patterns such as that shown in Figure 4 where four cracks initiate and progress from a center hole have been commonly observed in TMC specimens [4,7]. A finite element analysis conducted by John, et. al [19] found that the stress-intensity factor for fiber bridged matrix cracks in TMC (SCS-6/Ti-24-11) were reduced by 20% when dual parallel cracks similar to the schematics in Figure 4 were modeled compared to a single crack. In order model this effect in the current model, ΔK_m was multiplied by a correction factor for two parallel cracks [18]:

$$F_{par} = 1 - 0.293s\left(1-(1-s)^4\right) \tag{13}$$

where:

$$s = \frac{a}{a+h} \tag{14}$$

In this equation, a is the length of the cracks and h is the distance between the cracks. The measured values of h for each specimen are listed in Table 2. The values of F_{par} ranged from 1 to $1/\sqrt{2}$, which bound the value of 0.8 obtained by John, et. al [19] in their finite element analysis.

RESULTS AND DISCUSSIONS

The matrix crack growth behavior observed in the two TMC was analyzed using a FB model with thermal residual stresses. The frictional shear stress term τ in the FB model was used as a curve-fitting parameter to matrix crack growth data reduced using the crack growth law defined by Equation (1). The value of τ was determined for each of the three discrete-continuum relations: the MCE [8], MC [9] and ME [10] relations. Results are presented in the subsequent sections according to the lay-up and notch geometry. The effects of thermal residual stresses on the values of τ used in fiber bridging analysis are discussed.

Baseline Matrix Crack Growth Curves

The matrix crack growth curves used in the analysis for the Ti-15-3 and Timetal-21S materials are shown in Figures 5 and 6, respectively, with the corresponding material constants defined in Equation (1) . The value of m in Equation (1) represents the amount of shift in the crack growth curve due to the R-ratio. In order to evaluate m, crack growth data must be available for more than one R-ratio. For the two matrices considered in this study, the crack growth data was available for only one R-ratio, $R_m = 0.1$ Therefore, the value of m was calculated using Ti-6-4 crack growth data available at several R-ratios (unpublished data, R. Everett,

NASA Langley Research Center, 1993). It was assumed that the effect of R-ratio on the crack growth behavior would be the same for the three titanium alloys; thus, the same value of m was used.

Unidirectional Center Notch Specimens

The crack length as a function of the number of cycles at several applied stress levels was calculated using the value of τ which best fit the experimental results obtained in [6] for two center notched specimens of $[0]_8$ SCS-6/Ti-15-3 tested at room temperature, Figure 7. In both specimens, a single crack initiated and grew from each tip of the machined slit with no fiber breakage. For one specimen, the applied stress level was increased after a prescribed number of fatigue cycles, while for the other specimen, the applied stress was held constant. In the former case, the crack growth rate increased as the applied stress level increased. For both specimens, the crack growth rate decreased as the crack length increased due primarily to the observed fiber bridging phenomena.

As shown in Figure 7, when thermal residual stresses were included in the analysis, good agreement was obtained between the experiments (open symbols) and calculations (filled symbols) made using the MCE relations [8] and a single value of the frictional shear stress, τ = 20 MPa. These results are quite encouraging since the value of τ required to correlate the crack growth data when thermal residual stresses were neglected was a function of the applied stress level [6]. Similar results were obtained when the crack growth data was reduced using the MC [9] and the ME discrete-continuum relations [10]. A value of τ = 15 MPa was used for the MC relation and a value of τ = 60 MPa was used for the ME relation. For all three discrete-continuum relations considered, a single value of τ was sufficient to correlate the data when thermal residual stresses were included.

Using the same value of τ used to reduce the data shown in Figure 7, the debond or slip length as a function of distance from the first intact fiber was calculated and compared in Figure 8 to experimental results obtained in [6] for a center notched $[0]_8$ SCS-6/Ti-15-3 specimen. After fatigue loading, the surface of a specimen was polished to the mid plane of the outer ply of fibers. The mechanisms of fiber-matrix interfacial debonding were identified and the debond lengths were measured using the scanning electron microscope (SEM) [6]. Fiber-matrix debonding was assumed to exist where cracking between the carbon rich coatings and fracture of the brittle reaction zone was observed. The measured debond lengths were assumed to be equal to the entire damage process zone in the interface region.

In the FB model, the slip length is defined as the region over which the frictional shear stress acts. In the present study, the slip length is assumed to be equal to the debond length, and the measured debond lengths are compared to calculated slip lengths. As shown in Figure 8, good agreement was obtained between the measured and calculated debond length data using the value of τ used to consolidate the crack growth data in Figure 7. The calculations shown in Figure 8 were made using the MCE relation. When thermal residual stresses were

neglected, there was no correlation in the values of τ required to fit the debond length and crack growth data [6].

Cross-Ply Center Notch Specimen

The crack length as a function of the number of cycles at room temperature and at an elevated temperature of 200°C were calculated and plotted in Figure 9 using a value for τ which best fit the experimental results for two center notched specimens of $[0/90]_s$ SCS-6/Timetal-21S. In both cases, only one crack initiated and grew from each tip of the machined slit with no fiber breakage. As a result of the fiber bridging phenomena, the crack growth rate decreased as the crack length increased. The crack growth rate increased as the applied temperature increased.

As shown in Figure 9, good agreement was obtained between experiments (open symbols) and the calculations (filled symbols) using the MCE relations and values of τ = 50 MPa and 15 MPa for the room temperature and elevated temperature test results, respectively. For the elevated temperature test, the room temperature properties of the titanium matrix were used in the fiber bridging analysis. It was assumed that the mechanical properties of the matrix were the same at both temperatures since the modulus of Timetal-21S at 200°C was only 3% less than that at room temperature. Hence, the difference in the calculated crack growth behavior at the two temperatures is due primarily to the differences in thermal residual stress states which effects the calculated values of R_m and ΔK_m. Using the MC relation, τ = 50 MPa and τ = 15 MPa for the room temperature test and elevated temperature test, respectively. Using the ME relation, τ = 100 MPa and τ = 32 MPa for the room temperature test and elevated temperature test, respectively.

If the mechanical properties of the matrix are assumed to be identical at both temperatures, only R_m and ΔK_m affect the crack growth rate defined by Equation (1). At elevated temperatures, the axial thermal residual stress in the matrix σ_m^{Therm} is lower than at room temperature which results in lower values of R_m. For the room and elevated temperature tests, the calculated local R-ratios in the matrix were R_m = 0.75 and R_m = 0.64, respectively. From Equation (1), for a given value of ΔK_m, the crack growth rate increases with an increase in the value of R_m. Based solely on the values of R_m for the two test conditions, the crack growth rate should have been higher for the room temperature test than the elevated temperature test. Results shown in Figure 9, however, show the opposite trend; the crack growth rate data was higher for the elevated temperature test compared to the room temperature test.

Another factor affecting the crack growth rate is the stress-intensity factor range ΔK_m. Thermal residual stresses affect the value of ΔK_m. The lower value of τ for the elevated temperature test translated into a higher value in the stress-intensity factor range as shown in Figure 10. At the elevated temperature, the value of ΔK_m was higher than at room temperature. Using the crack growth law defined by Equation (1), for a given value of R_m,

the crack growth rates increases with an increase in the value of ΔK_m which agrees with the results shown in Figure 9. As a result of the lower thermal residual stresses at the elevated temperature test, the value of ΔK_m increased while the value of R_m decreased. The lower values of τ for the elevated temperature results suggests that the radial thermal residual stresses acting across the debonded fiber-matrix interfaces in the 0° plies were lower. These radial stresses "choke" the fibers which enhances the shear transfer between the fiber and matrix. By lowering the radial thermal stresses, the amount of shear transfer and displacement constraint between the fiber and matrix were lowered thereby increasing the stress-intensity factor. The increase in the value of ΔK_m had a more profound effect on the crack growth rate than the decrease in the value of R_m.

Cross-Ply Center Hole Specimen

The crack length as a function of the number of cycles at several applied stress levels was calculated using a value for τ which best fit the experimental results obtained in [7] for room temperature tests of cross-ply SCS-6/Ti-15-3 and SCS-6/Timetal-21S laminates as shown in Figures 11 and 12, respectively. The calculations shown in Figures 11 and 12 were reduced using the MCE relation. As shown in these figures, when the thermal residual stresses were included in the analysis, good agreement was obtained between the calculations (filled symbols) and the experiments (open symbols) using a single value of the frictional shear stress for each laminate, τ = 10 MPa and τ = 50 MPa, respectively. Using the MC relation, the values of frictional shear stress needed to fit the data were τ = 10 MPa and τ = 50 MPa for the SCS-6/Ti-15-3 and SCS-6/Timetal-21S laminates, respectively. Using the ME relation, the values of frictional shear stress needed to fit the data were τ = 25 MPa and τ = 100 MPa for the SCS-6/Ti-15-3 and SCS-6/Timetal-21S, respectively.

Effect of Thermal Residual Stress on the Frictional Shear Stress

The effect of thermal residual stresses on fiber bridging analysis is shown by the values of the frictional shear stress term required to reduce the crack growth data, listed in Table 2. The values of τ listed in this table were determined using the ME relations with and without thermal residual stress. For the unidirectional SCS-6/Ti-15-3 specimens tested in [6], the value of τ required to fit crack growth data varied from 12 MPa to 41 MPa when thermal residual stresses are neglected (i.e. original fiber bridging analysis). However, when thermal residual stresses were included in the analysis, a single value of frictional shear stress, τ = 60 MPa, was able to fit the data. Thus, for a given material system, lay-up, and temperature, a single value of τ was sufficient to analyze the crack growth data. Thermal residual stresses are an important factor not included in the original formulations of the FB models.

CONCLUDING REMARKS

Thermal residual stresses were implemented into the analysis of fiber-bridged matrix crack growth in notched titanium matrix composites (TMC). The matrix crack growth behavior in unidirectional and cross-ply SCS-6/Ti-15-3 and SCS-6/Timetal-21S laminates containing center holes or center notches was analyzed. Results from the analysis revealed that tensile axial stresses in the matrix were induced during composite fabrication and heat treatment resulting in higher constituent R-ratios in the matrix (i.e., ratio of stresses at the minimum and maximum applied loads) compared to the continuum R-ratio based on the applied load (i.e., ratio of the minimum and maximum applied load). Thus, the continuum R-ratio of the applied load is not appropriate in the analysis of fiber-bridged matrix crack growth; the R-ratio based on the matrix stresses should be used since the crack growth does indeed take place in the matrix material.. Thermal residual stresses were incorporated in the formulation of a fiber bridging (FB) model which combines a continuum fracture mechanics approach and a micromechanics approach to yield stress intensity factor solutions for fiber bridged matrix cracks. The frictional shear stress term τ assumed in the FB model was used as a fitting parameter to matrix crack growth data.

Tension-tension fatigue tests were conducted at room temperature and at an elevated temperature of 200°C. For a given material system, and lay-up, and temperature, a single value of τ was sufficient to reduce the crack growth data. The crack growth rates were higher for the elevated temperature test compared to the room temperature test. The fiber-bridging analysis indicated that the increase in crack growth rates was due to the lower thermal residual stresses which resulted in an increase in the stress-intensity factor range in the matrix. Incorporation of the residual thermal stresses showed their effects in two significant ways: (1) The stress ratio in the matrix increases by including the effects of residual stresses over that of the applied stress ratio. The residual stress in the matrix is a function of the fiber volume fraction and lay-up. Therefore these variations will be reflected in the matrix stress ratio. (2) The residual stresses change as a function of temperature. The axial stress ratio in the 0° ply matrix material goes down as would the radial residual stresses as the temperature is increased. The effect of the lowered radial stresses is to directly lower τ because less frictional stress will be transferred between the matrix and fiber. When testing at elevated temperatures, it was found in this study that the lowering of the frictional shear stress τ due to the decrease in radial residual stresses is more profound than the lowering of the stress ratio in the matrix material.

Results from this study showed that thermal residual stresses are an important fundamental factor that was lacking in the original FB models. By including thermal residual stresses in the FB model, fiber bridging analysis more accurately models the fiber bridging phenomena observed in TMC.

Acknowledgments

The first author gratefully acknowledges the support extended by the National Research Council, Washington, DC., through their Associateship Program, while conducting this

research. The crack growth data for the neat Timetal-21S matrix material was obtained from R. John and N. E. Ashbaugh, University of Dayton Research Institute, 1992. The Ti-6-4 data used to estimate the shift factor *m* was obtained from R. Everett, NASA Langley Research Center, 1993.

REFERENCES

[1] Hillberry, B. M. and Johnson, W. S., "Fatigue Crack Spacing in the Matrix of a Continuous Fiber SCS-6/Ti Composite," *Journal of Composites Technology and Research,* JCTRER, Vol. 15, No. 3, Fall 1993, pp. 210-216.

[2] Naik, R. A., and Johnson, W. S., "Observations of Fatigue Crack Initiation and Damage Growth in Notched Titanium Matrix Composites," *Third Symposium on Composite Materials: Fatigue and Fracture, ASTM STP 1110,* T. K. O'Brien, Ed., American Society for Testing and Materials, 1991, pp. 753-771.

[3] Harmon, D. M., and Saff, C. R.,"Damage Initiation and Growth in Fiber Reinforced Metal Matrix Composites," *Metal Matrix Composites: Testing, Analysis and Failure, ASTM STP 1032,* W.S. Johnson, Ed., American Society for Testing and Materials, 1989, pp. 237-250.

[4] Bakuckas, J. G. Jr., Johnson, W. S., and Bigelow, C. A.,"Fatigue Damage in Cross-Ply Titanium Metal Matrix Composites Containing Center Holes," *Journal of Engineering Materials and Technology,* Vol. 115, October 1993, pp. 404-410.

[5] Kantzos, P. and Telesman, J., "Fatigue Crack Growth Study of SCS6/Ti-15-3 Composite," *Int. J. Fatigue,* Vol 12, No. 5, September 1990, pp. 409-415.

[6] Bakuckas, J. G., Jr., and Johnson, W. S.,"Application of Fiber Bridging Models to Fatigue Crack Growth in Unidirectional Titanium Metal Matrix Composites," *Journal of Composites Technology and Research,* Vol. 15, No. 3, Fall 1993, pp. 242-255.

[7] Bakuckas, J. G., Jr., and Johnson, W. S.,"Modeling Fatigue Crack Growth in Cross Ply Titanium Matrix Composites," NASA TM 108988, National Aeronautics and Space Administration, Washington, D.C., 1993, pp.35.

[8] Marshall, D. B., Cox, B. N., and Evans, A. G., "The Mechanics of Matrix Cracking in Brittle-Matrix Fiber Composites," *Acta Metall.,* Vol. 33, No. 11, 1985, pp. 2013-2021.

[9] McCartney, L. N., "Mechanics of Matrix Cracking in Brittle-Matrix Fibre-Reinforced Composites," *Proc. R. Soc. Lond.,* A 409, 1987, pp. 329-350.

[10] McMeeking, R. M., and Evans, A. G., "Matrix Fatigue Cracking in Fiber Composites," *Mechanics of Materials,* Vol. 9, 1990, pp. 217-227.

[11] Bower, A. F., and Ortiz, M., "A Three-Dimensional Analysis of Cracks Trapping and Bridging By Tough Particles," *J. Mech. Phys. Solid.,* Vol. 39, No. 6, 1991, pp. 815-858.

[12] Walker, W., "The Effect of Stress Ratio During Crack Propagation and Fatigue for 2024-T3 and 7075-T6 Aluminum," *Effects of Environment and Complex Load History on Fatigue Life, ASTM STP 462*, American Society for Testing and Materials, 1970, pp. 1-14.

[13] Mirdamadi, M., Johnson, W. S., Bahei-El-Din, Y. A., and Castelli, M. G., "Analysis of Thermomechanical Fatigue of Unidirectional Titanium Matrix Composites," *Composite Materials: Fatigue and Fracture, Fourth Volume*, ASTM STP 1156, W.W. Stinchomb and N.E. Ashbaugh, Eds., Philadelphia, 1993, pp. 591-607.

[14] Mirdamadi, M., and Johnson, W. S., "Prediction of Stress-Strain Response of SCS-6/Timetal-21S Subjected to the Hypersonic Flight Profile" NASA TM 109026, National Aeronautics and Space Administration, Washington, D.C., February 1994.

[15] Lekhnitskii, S. G., *Theory of Elasticity of an Anisotropic Body*, Holden-Day, San Francisco, 1963.

[16] Newman, J. C., Jr., "A Nonlinear Fracture Mechanics Approach to the Growth of Small Cracks," *Behavior of Short Cracks in Airframe Components*, AGARD Conference Proceedings No. 328, 1982, pp. 6.1 - 6.26.

[17] Newman, J. C., Jr., "An Improved Method of Collocation for the Stress Analysis of Cracked Plates with Various Shaped Boundaries," *NASA TN D-6376*, National Aeronautics and Space Administration, Washington, D.C., 1971.

[18] Tada, H., Paris, P. C., and Irwin, G. R., *The Stress Analysis of Cracks Handbook*, Del Research Corporation, St. Louis, MO, 1985.

[19] John, R., Jira, J. R., Larsen, J. M., and Ashbaugh, N. E., "Analysis of Bridged Fatigue Cracks in Unidirectional SCS-6/Ti-24Al-11Nb Composite," *Fatigue '93 Vol II*, Bailon and Dickson, Eds., Chameleon Press, London, ,1993, pp. 1091-1096.

[20] Lenning, G. A, Hall, J. A., Rosenblum, M. E., and Trepel, W. B., "Cold Formable Titanium Sheet," *AFWAL-TR-82-4174*, December 1982.

Table 1. Material Properties:

		Material System	
	Property	**SCS-6/Ti-15-3**	**SCS-6/Timetal-21S**
Matrix	E_m (GPa)	92.4	116.0
	ν_m	0.34	0.34
	C	3.8E-11	5.5E-11
	n	2.8	2.5
	m	0.35	0.35
	α_m mm/mm/C	9.7×10^{-6}	8.6×10^{-6}
Fiber:	E_f (GPa)	400.0	400.0
	ν_f	0.25	0.25
	α_f mm/mm/C	3.6×10^{-6}	3.6×10^{-6}
Composite:	Lay-Up	$[0]_8$	$[0/90]_s$
	ν_f	0.33	0.36
	E_L (GPa) [a]	192.2	188.4
	E_T (GPa) [a]	130.1	188.4
	G_{LT} (GPa) [a]	45.9	58.1
	ν_{LT} [a]	0.32	0.26
	$\sigma_m^{Thermal}$ (MPa) [a]	202.0 [b]	221.9 [c]
	Lay-Up	$[0/90]_s$	$[0/90]_{2s}$
	ν_f	0.35	0.38
	E_L (GPa) [a]	168.4	192.9
	E_T (GPa) [a]	168.4	192.9
	G_{LT} (GPa) [a]	47.4	59.3
	ν_{LT} [a]	0.25	0.26
	$\sigma_m^{Thermal}$ (MPa) [a]	183.8 [b]	230.5 [c]

[a] Predicted using VISCOPLY [13] based on constituent properties
[b] Axial ,thermal residual stress in matrix in 0° plies for cool-down from 555°C
[c] Axial ,thermal residual stress in matrix in 0° plies for cool-down from 620°C

Table 2. Specimen loading history and fiber bridging analysis parameters:

Material	Lay-Up	Spec. Type	S_{max} (MPa)	2a/W	R_m	h (mm)	Temp. (°C)	τ (MPa)[a]	τ (MPa)[b]
SCS-6/Ti-15-3	$[0]_8$	Center Notch	120	0.30	0.79	N.A.[c]	21	60	12 [6]
SCS-6/Ti-15-3	$[0]_8$	Center Notch	200	0.30	0.71	N.A.	21	60	20 [6]
SCS-6/Ti-15-3	$[0]_8$	Center Notch	300	0.30	0.62	N.A.	21	60	20 [6]
SCS-6/Ti-15-3	$[0]_8$	Center Notch	325	0.35	0.62	N.A.	21	60	40 [6]
SCS-6/Ti-15-3	$[0/90]_s$	Center Hole	150	0.35[d]	0.71	2.8	21	25	11 [7][e]
SCS-6/Ti-15-3	$[0/90]_s$	Center Hole	200	0.35[d]	0.65	2.1	21	25	11 [7][e]
SCS-6/Ti-15-3	$[0/90]_s$	Center Hole	250	0.35[d]	0.61	2.0	21	25	7 [7][e]
SCS-6/Timetal-21S	$[0/90]_s$	Center Hole	125	0.35[d]	0.77	1.5	21	100	30 [7][e]
SCS-6/Timetal-21S	$[0/90]_s$	Center Notch	150	0.20	0.75	N.A.	21	100	-
SCS-6/Timetal-21S	$[0/90]_s$	Center Notch	150	0.20	0.64	N.A.	200	32	-
SCS-6/Timetal-21S	$[0/90]_{2s}$	Center Hole	150	0.32[d]	0.74	1.9	21	100	35 [7][e]
SCS-6/Timetal-21S	$[0/90]_{2s}$	Center Hole	200	0.32[d]	0.69	2.0	21	100	35 [7][e]

a Frictional shear stress required to analyze data using ME relations [10] when thermal residual stresses are considered

b Frictional shear stress required to analyze data using ME relations [10] when thermal residual stresses are neglected

c Not applicable

d Hole diameter to width ratio (d/W)

e Frictional shear stress required to analyze data using ME relations [10] neglecting the effect of parallel cracks

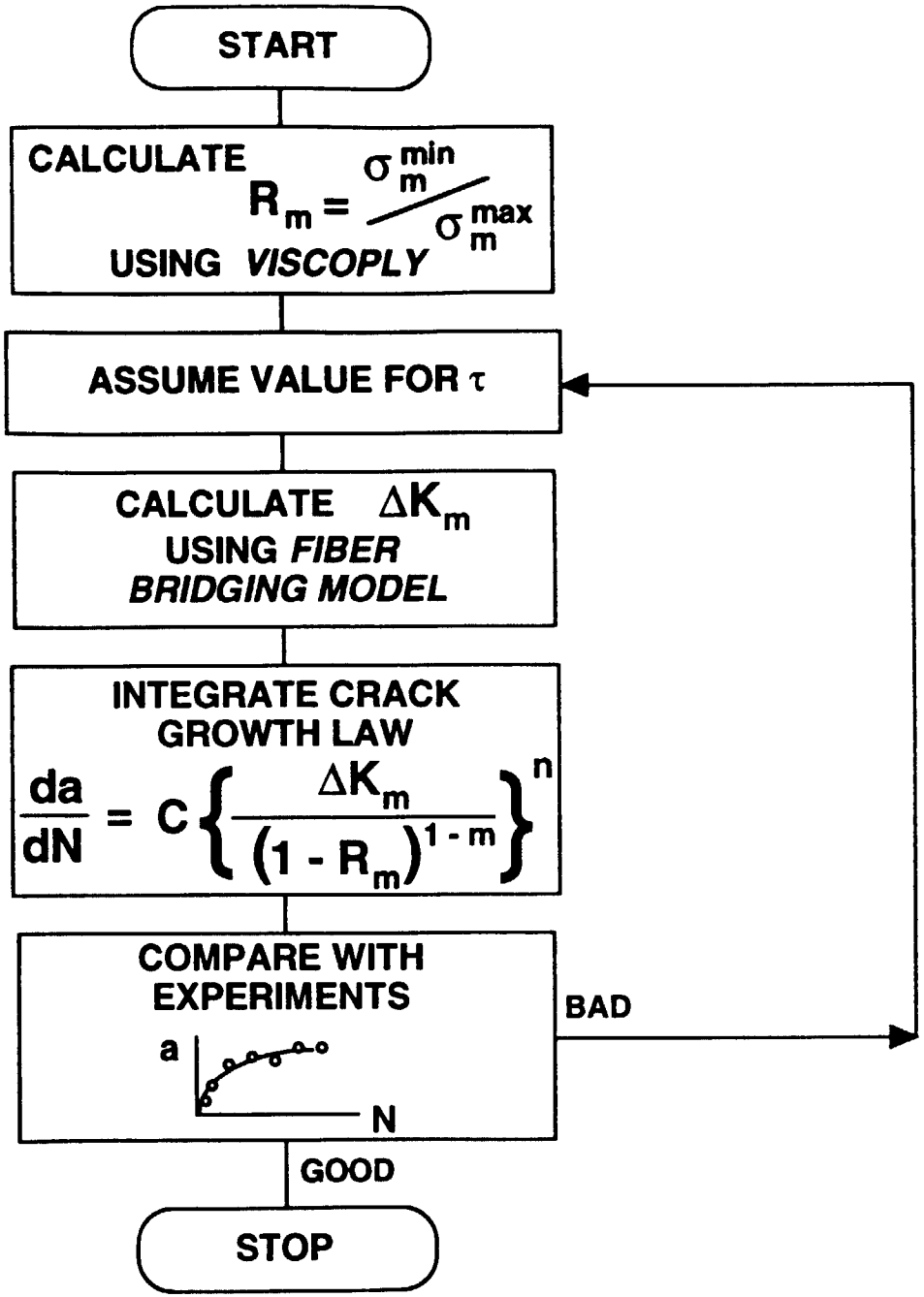

Figure 1. Analysis of fiber-bridged matrix cracks

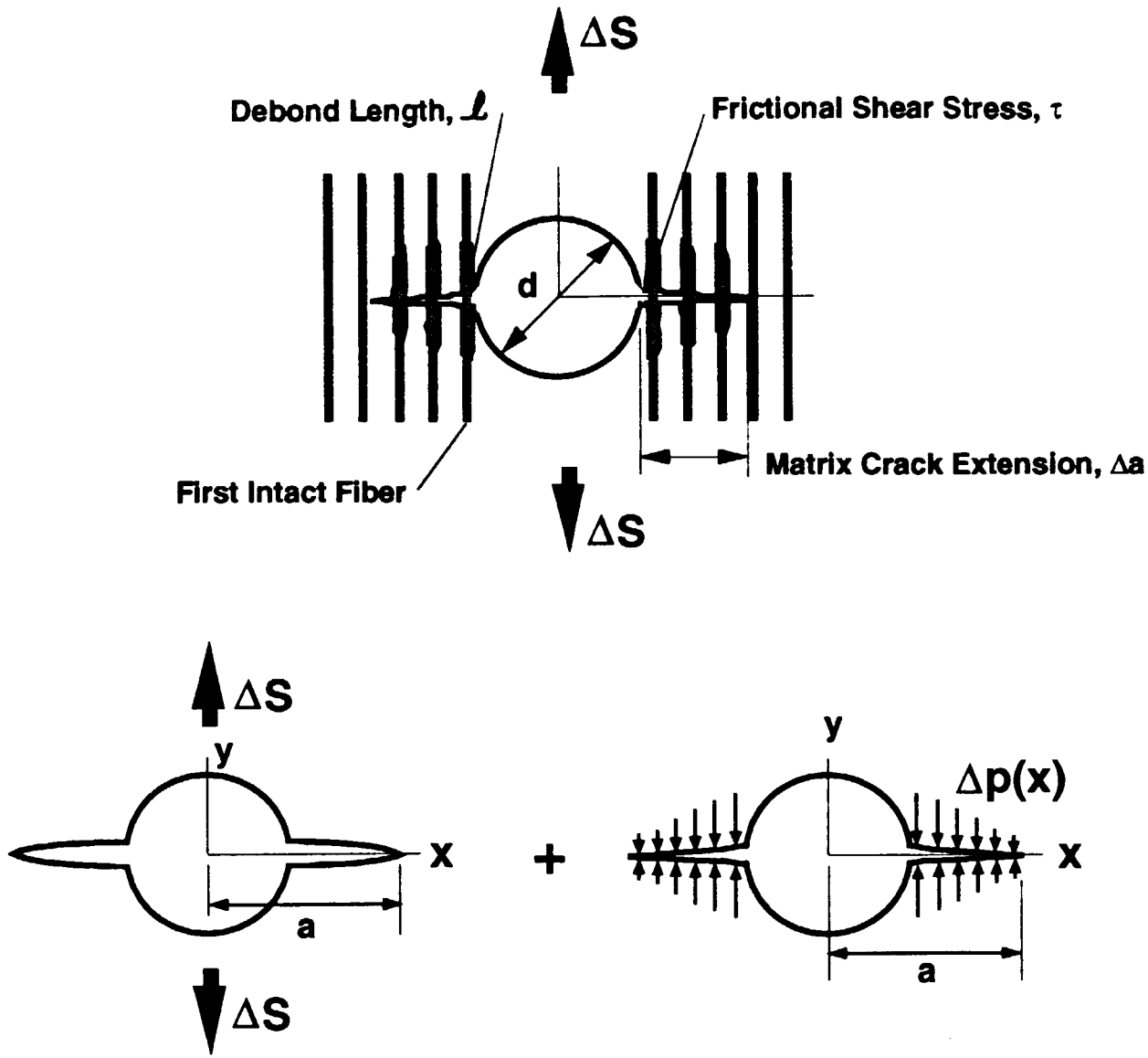

Figure 2. Continuum fracture mechanics approximation of matrix crack growth process. Fibers bridging crack are idealized as a closure pressure. Governing equation is formulated by superposition of a crack subjected to a far-field applied stress and a crack subjected to a closure pressure.

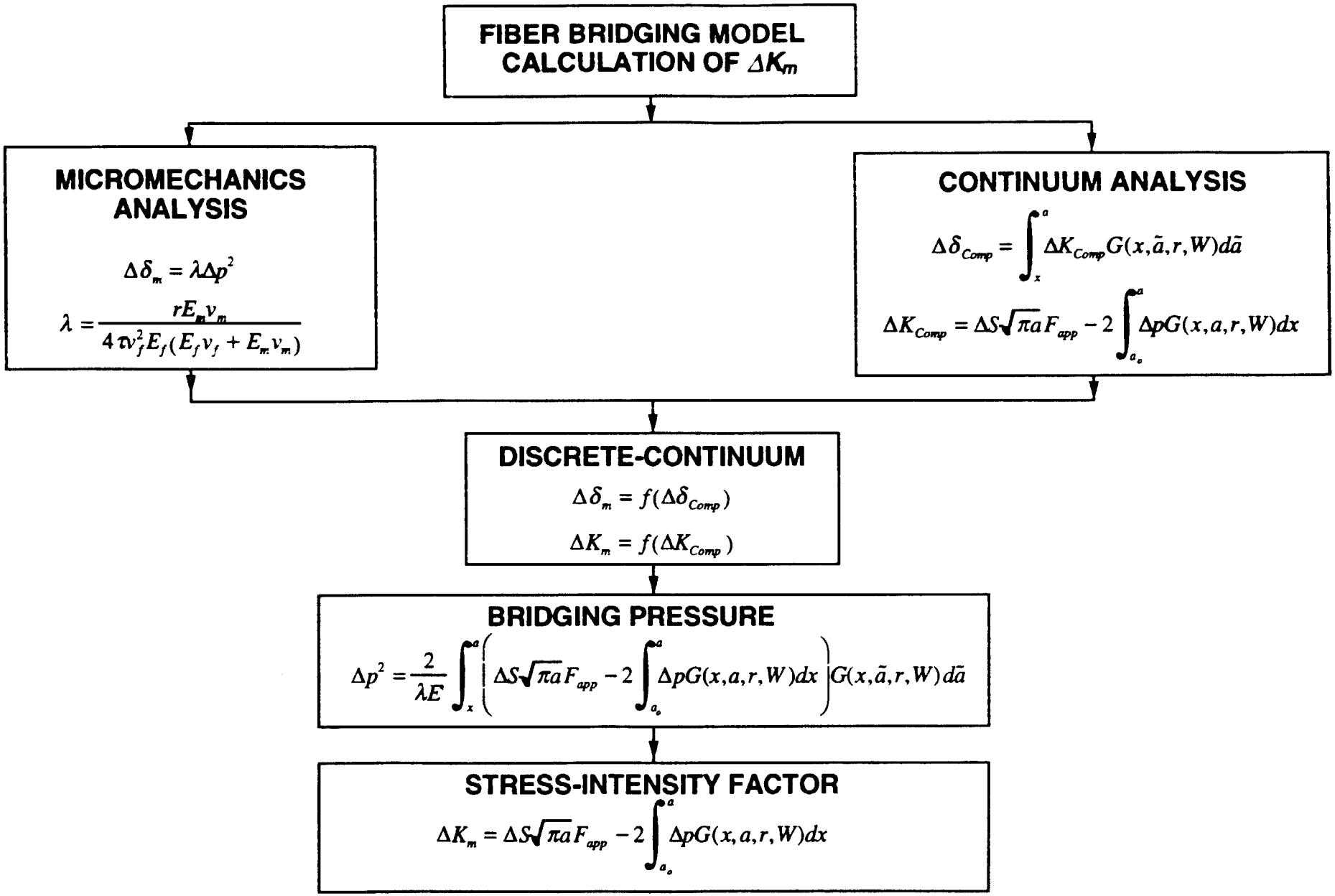

Figure 3. Calculation of Stress-Intensity Factor using Fiber Bridging Model

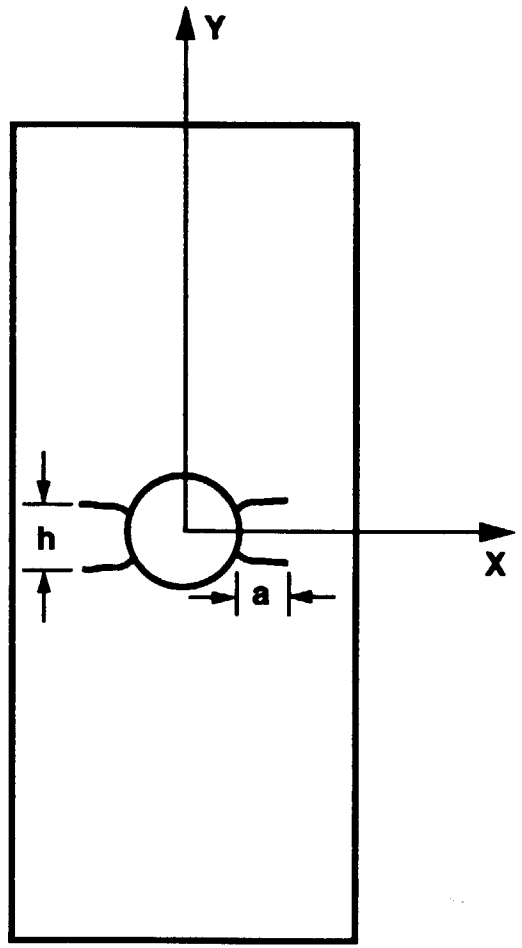

Figure 4. Schematics of cracking pattern commonly observed in TMC containing center hole.

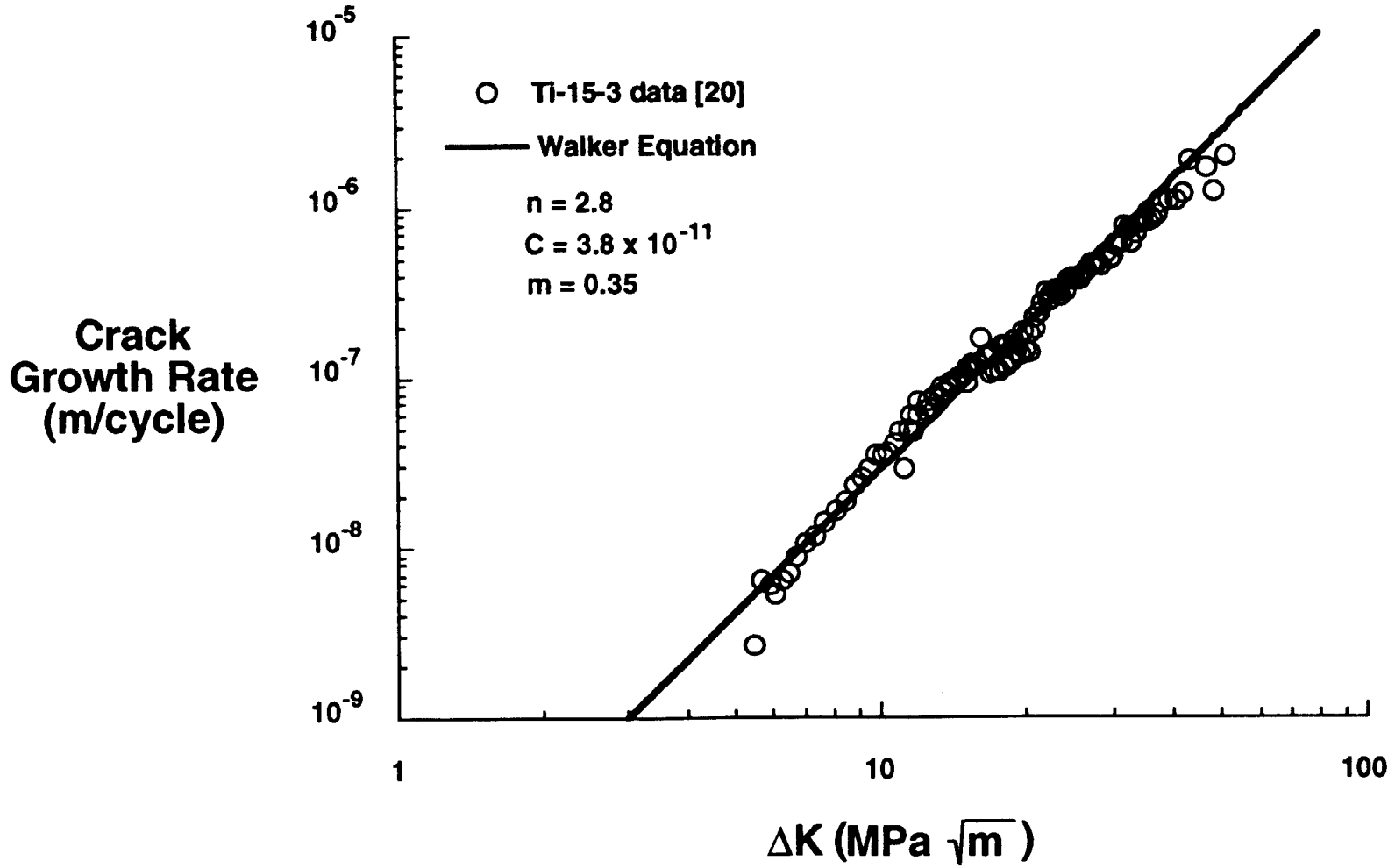

Figure 5. Room temperature crack growth rate data for Ti-15-3. R-ratio = 0.1.

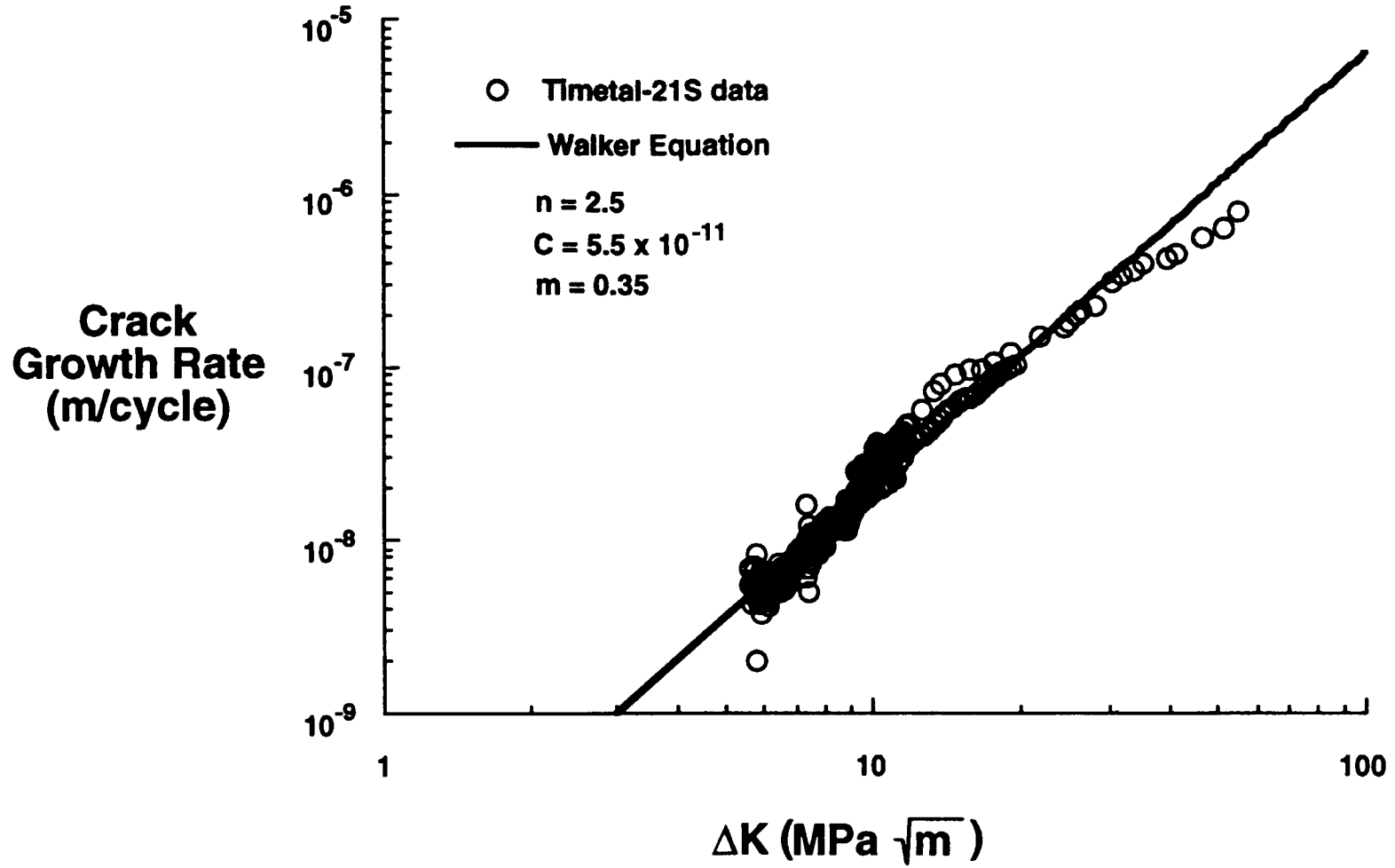

Figure 6. Room temperature crack growth rate data for Timetal-21S. R-ratio = 0.1.

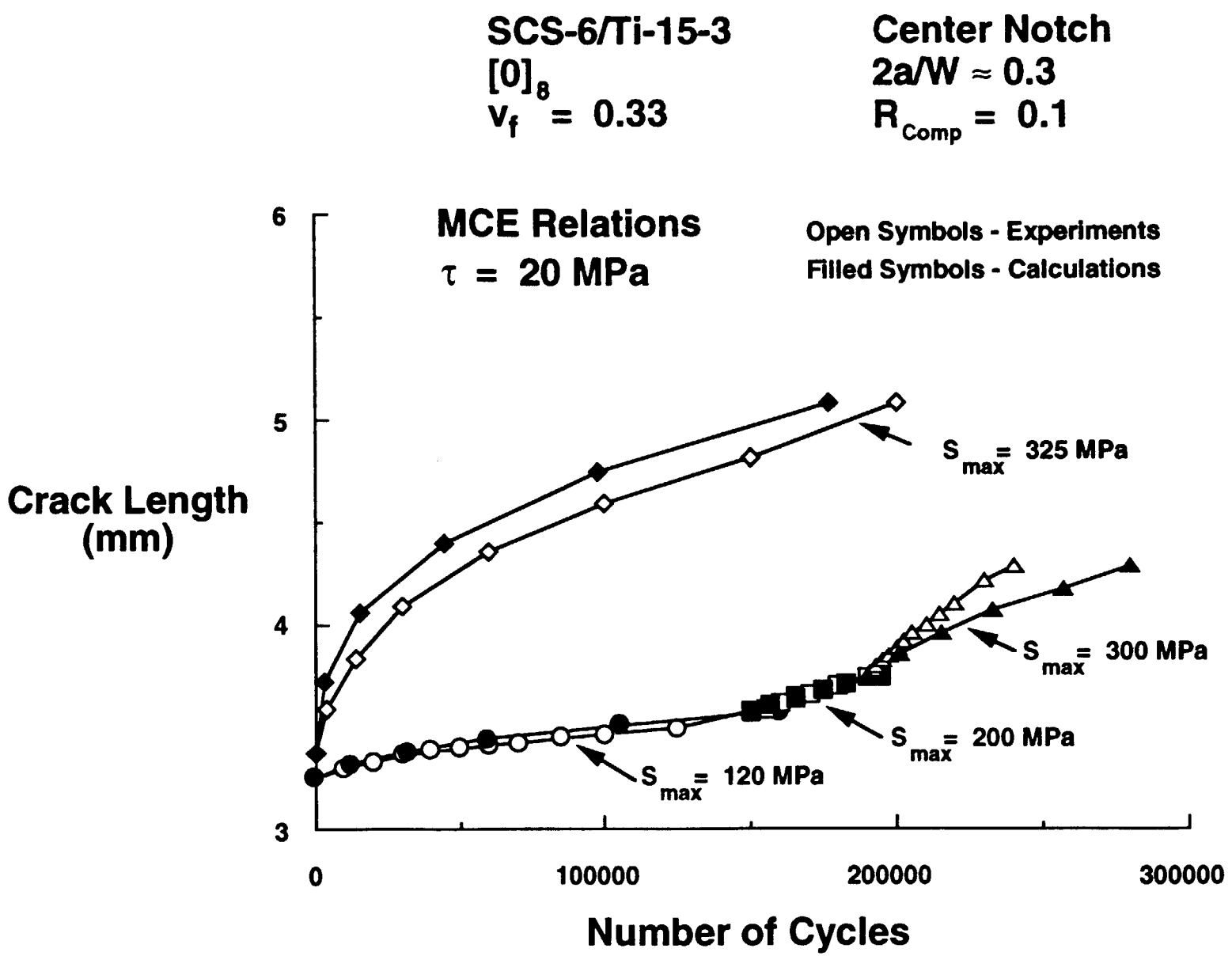

Figure 7. Crack growth data for center notched $[0]_8$ SCS-6/Ti-15-3 laminates at several applied stress levels. Comparison between experiments and calculations made using Fiber Bridging Model.

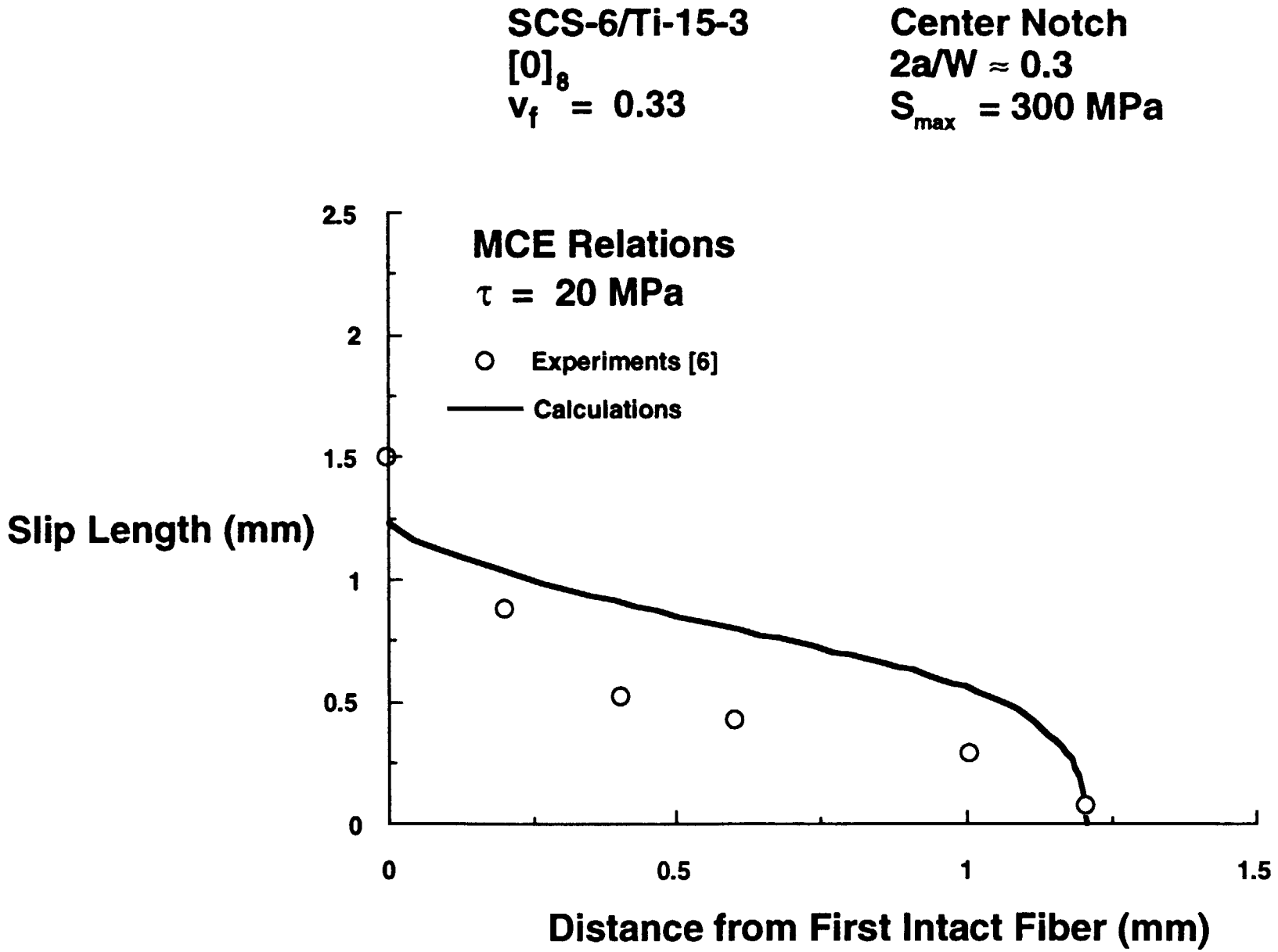

Figure 8. Debond length data for a center notched $[0]_8$ SCS-6/Ti-15-3 specimen subjected to 50,000 cycles. Comparison between experiments and calculations made using Fiber Bridging Model.

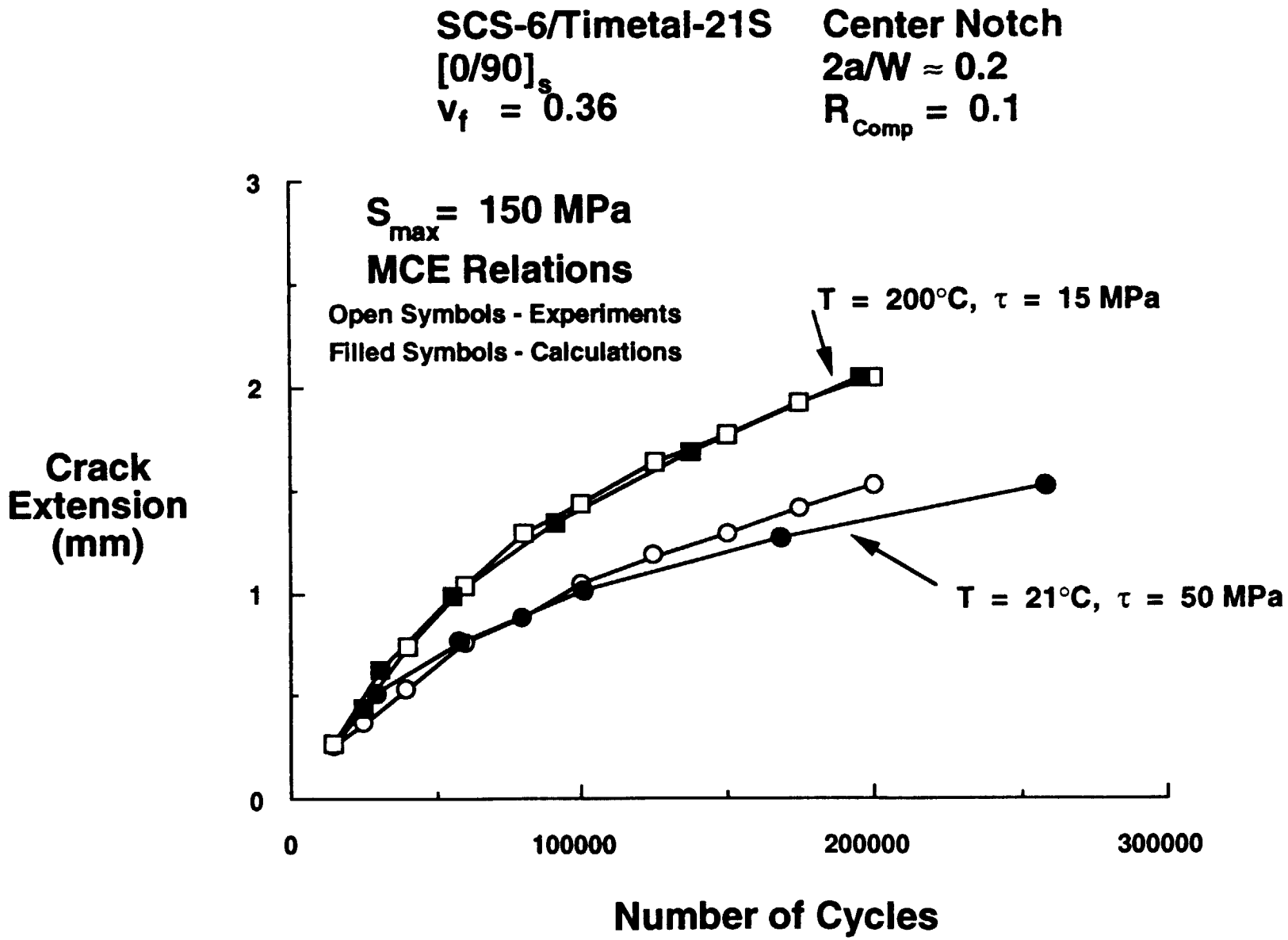

Figure 9. Crack growth data for center notched $[0/90]_s$ SCS-6/Timetal-21S laminates at two temperature levels. Comparison between experiments and calculations made using Fiber Bridging Model.

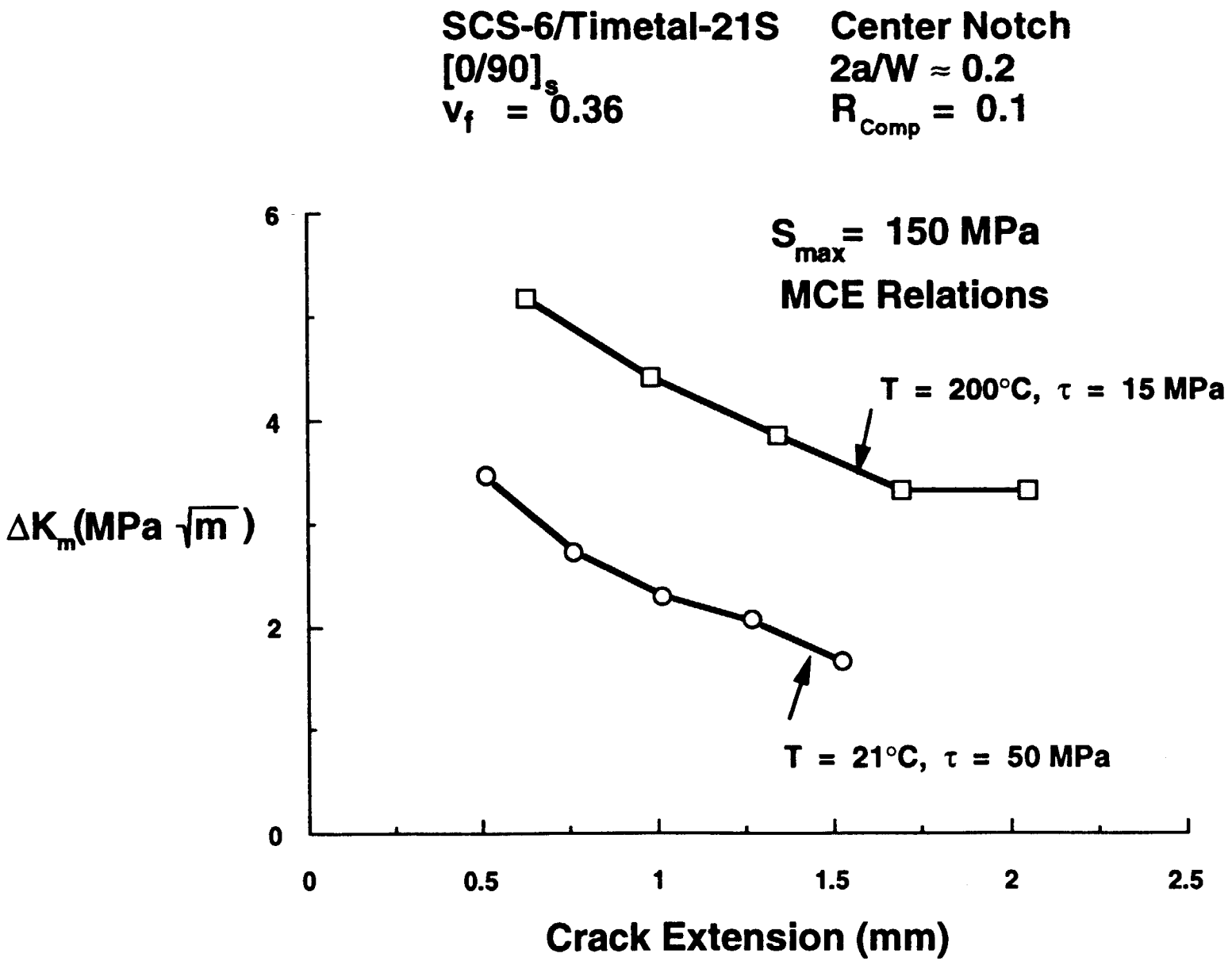

Figure 10. Variation of stress intensity with crack extension in center notched $[0/90]_s$ SCS-6/Timetal-21S laminates at two temperature levels.

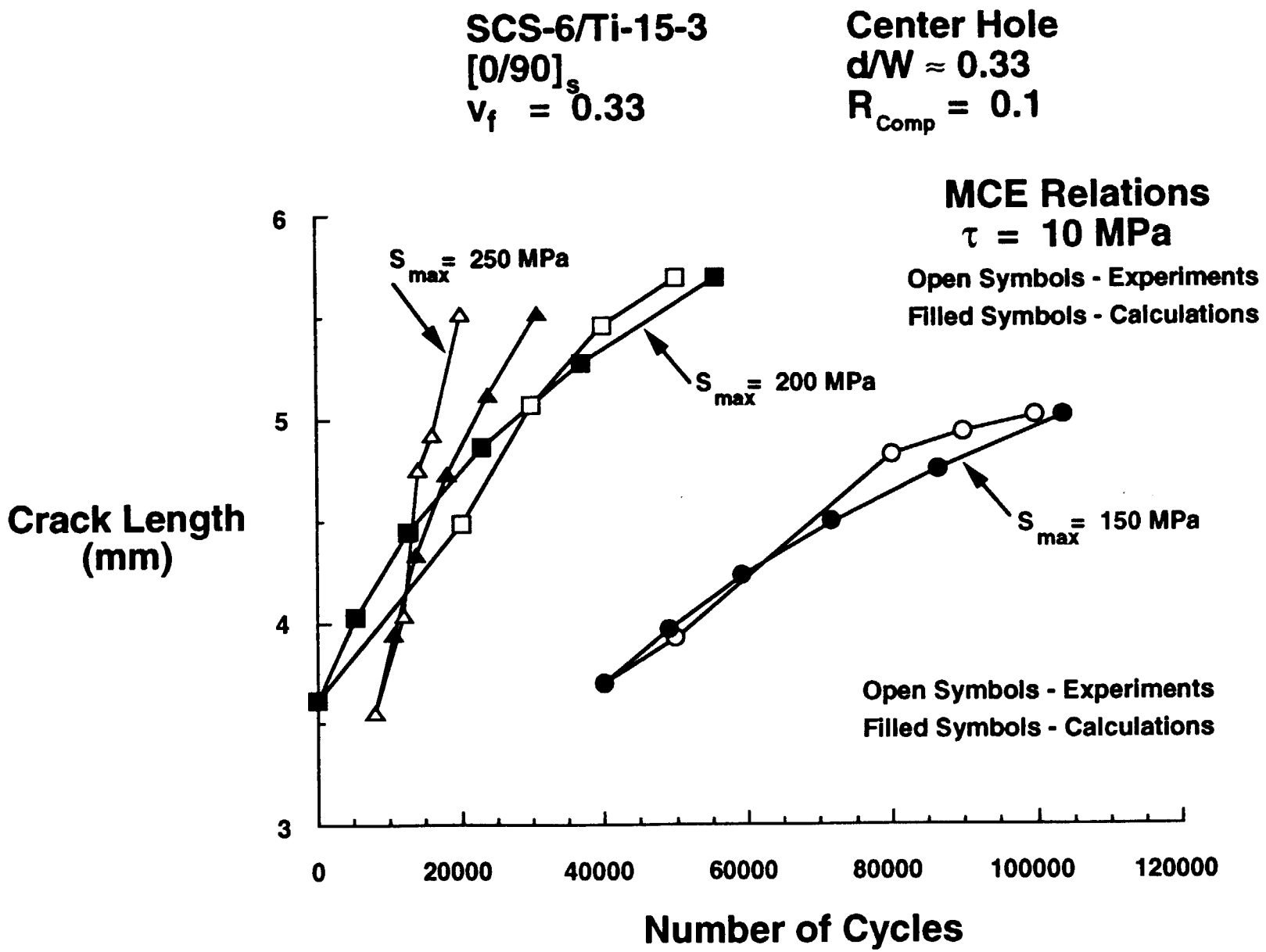

Figure 11. Crack growth data for center hole $[0/90]_s$ SCS-6/Ti-15-3 laminates at several applied stress levels. Comparison between experiments and calculations made using Fiber Bridging Model.

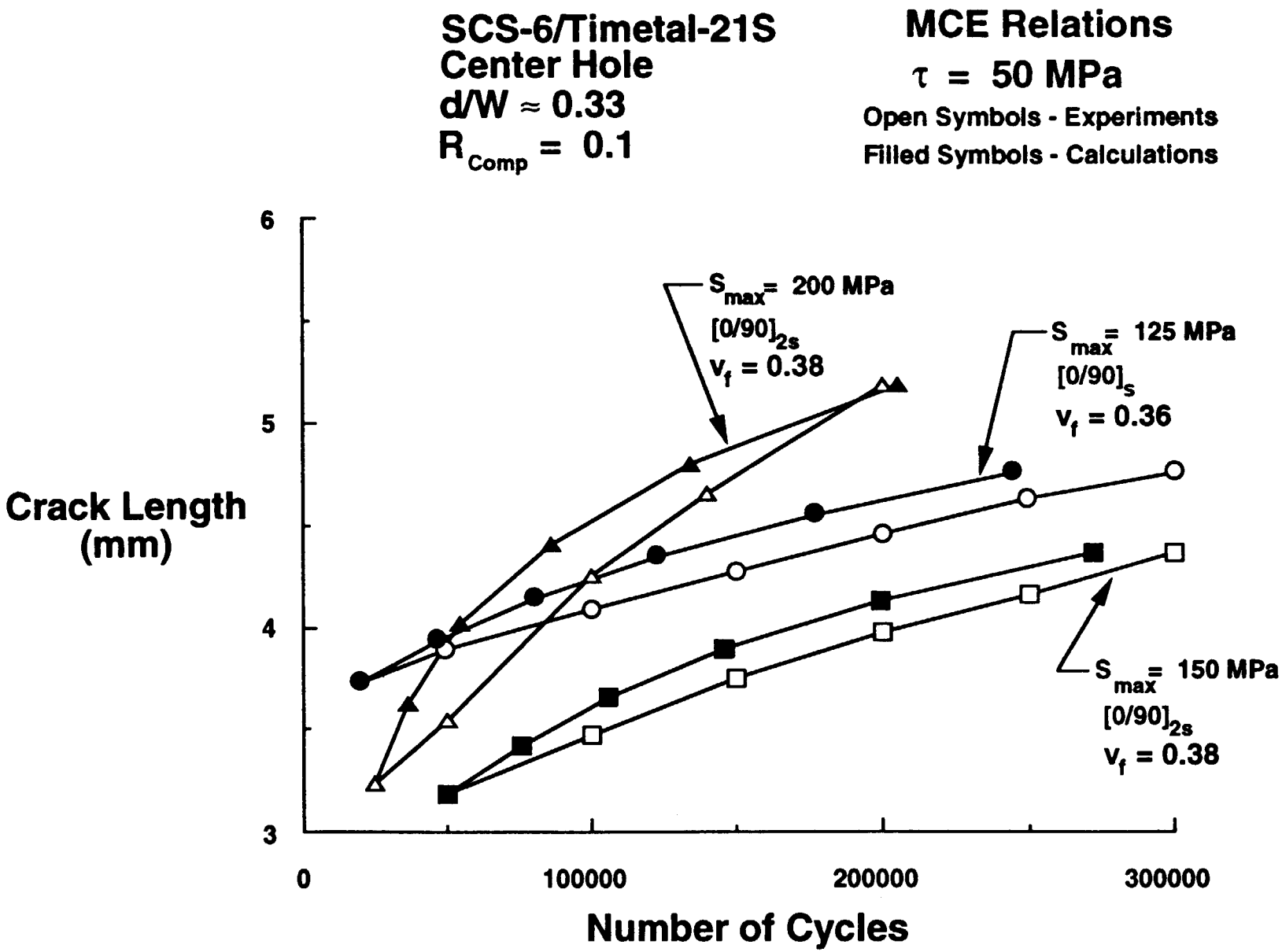

Figure 12. Crack growth data for center hole cross-ply SCS-6/Timetal-21S laminates at several applied stress levels. Comparison between experiments and calculations made using Fiber Bridging Model.

APPENDIX A - MICROMECHANICS OF FIBER BRIDGING

The relation between the crack opening displacement and the bridging pressure is derived in detail for each region of fatigue loading shown in Figure A1a. A free body diagram of a fiber in the wake of the matrix crack for each loading phase is shown in Figures A1b and A1c. A constant temperature change, $\Delta T'$, was applied prior to the mechanical loading.

Loading: O-A

During the initial loading along O-A (Figure A1a), the frictional shear stress, τ, is constant in the slip region, ℓ, and opposes the fiber stress, Figure A1b. This free body diagram is constructed assuming the maximum load is just reached (Point A in Figure A1a). Along line BB' (end of slip region), the strains in the fiber and the matrix are equal:

$$\frac{\left(\sigma_f^{BB'}\right)^{max}}{E_f} = \frac{\left(\sigma_m^{BB'}\right)^{max}}{E_m} \tag{A1}$$

where $\left(\sigma_f^{BB'}\right)^{max}$ and $\left(\sigma_m^{BB'}\right)^{max}$ are the fiber and matrix stresses along line BB' at the maximum applied load (Point A in Figure A1a). Overall equilibrium in the matrix in the slip region requires:

$$\left(\sigma_m^{BB'}\right)^{max} A_m - 2\pi r\tau\ell = 0 \tag{A2}$$

where A_m is the cross-sectional area of the matrix. Equilibrium in the fiber in the slip region requires:

$$\left(\sigma_f^{BB'}\right)^{max} A_f + 2\pi r\tau\ell = \left(\sigma_f^{AA'}\right)^{max} A_f \tag{A3}$$

where $\left(\sigma_f^{AA'}\right)^{max}$ is the fiber stress along the matrix crack centerline AA' and A_f is the cross-sectional area of the fiber. Combining Equations (A1), (A2), and (A3), the fiber stress along the crack centerline AA' at the maximum load is:

$$\left(\sigma_f^{AA'}\right)^{max} = \frac{2\tau\ell}{r}\eta \tag{A4}$$

where:

$$\eta = \left(1 + \frac{E_f \nu_f}{E_m \nu_m}\right) \tag{A5}$$

The total extension of the matrix in the slip region due to the mechanical and thermal loading:

$$u^{max} = \int_0^{\ell} \left(\frac{\left(\sigma_m^{BB'}\right)^{max}}{E_m} - \frac{2\pi\tau r y}{E_m A_m} \right) dy + \alpha_m \Delta T \ell = \frac{\pi\tau r \ell^2}{E_m A_m} + \alpha_m \Delta T \ell \tag{A6}$$

and of the fiber:

$$\frac{\delta_m^{max}}{2} + u^{max} = \int_0^{\ell} \left(\frac{\left(\sigma_f^{BB'}\right)^{max}}{E_f} + \frac{2\pi\tau r y}{E_f A_f} \right) dy + \alpha_f \Delta T \ell =$$

$$\frac{\left(\sigma_f^{BB'}\right)^{max} \ell}{E_f} + \frac{\pi\tau r \ell^2}{E_f A_f} + \alpha_f \Delta T \ell \tag{A7}$$

Combining Equations (A1), (A2), (A6), and (A7), the crack opening displacement at the maximum load, δ_m^{max}:

$$\frac{\delta_m^{max}}{2} = \frac{\tau \ell^2}{E_f r} \eta + \Delta T \ell \left(\alpha_f - \alpha_m\right) \tag{A8}$$

Substituting Equation (A4) into (A8) yields the relation between the fiber stress along the crack centerline and the discrete crack opening displacement at the maximum applied load:

$$\frac{\delta_m^{max}}{2} = \frac{r\left(\left(\sigma_f^{AA'}\right)^{max}\right)^2}{4\tau E_f \eta} + \frac{\Delta T r \left(\sigma_f^{AA'}\right)^{max}}{2\tau\eta} \left(\alpha_f - \alpha_m\right) \tag{A9}$$

Unloading: A-B

Upon unloading, the frictional shear stress reverses direction within a length, ℓ_R, in the slip region. The free body diagram, Figure A1c, is constructed assuming the minimum load is just reached (Point B in Figure A1a). The procedure to determine the relation between the fiber stress and discrete crack opening displacement is similar to that at maximum load. Along line BB' (end of slip region), the strains in the fiber and the matrix are equal:

$$\frac{\left(\sigma_f^{BB'}\right)^{\min}}{E_f} = \frac{\left(\sigma_m^{BB'}\right)^{\min}}{E_m} \tag{A10}$$

Overall equilibrium in the matrix in the slip region requires:

$$\left(\sigma_m^{BB'}\right)^{\min} A_m - 2\pi\tau r\left(\ell - \ell_R\right) + 2\pi\tau r\ell_R = 0 \tag{A11}$$

and in the fiber:

$$\left(\sigma_f^{BB'}\right)^{\min} A_f + 2\pi\tau r\left(\ell - \ell_R\right) - 2\pi\tau r\ell_R = \left(\sigma_f^{AA'}\right)^{\min} A_f \tag{A12}$$

Combining Equations (A10), (A11), and (A12), the fiber stress along the crack centerline at the minimum load is:

$$\left(\sigma_f^{AA'}\right)^{\min} = \frac{2\pi\tau\eta}{r}\left(\ell - 2\ell_R\right) \tag{A13}$$

Substituting Equation (A4) into (A13):

$$\Delta\sigma_f^{AA'} = \frac{4\pi\tau\eta}{r}\ell_R \tag{A14}$$

where $\Delta\sigma_f^{AA'} = \left(\sigma_f^{AA'}\right)^{\max} - \left(\sigma_f^{AA'}\right)^{\min}$. The total extension of the matrix in the slip region at the minimum load is:

$$u^{\min} = \int_0^{\ell-\ell_R}\left(\frac{\left(\sigma_m^{BB'}\right)^{\min}}{E_m} - \frac{2\pi\tau ry}{E_m A_m}\right)dy +$$

$$\int_{\ell-\ell_R}^{\ell}\left(\frac{\left(\sigma_m^{BB'}\right)^{\min}}{E_m} - \frac{4\pi\tau r\left(\ell-\ell_R\right)}{E_m A_m} + \frac{2\pi\tau ry}{E_m A_m}\right)dy + \alpha_m \Delta T\ell \tag{A15}$$

which reduces to:

$$u^{\min} = \frac{\left(\sigma_m^{BB'}\right)^{\min}\ell}{E_m} + \frac{\pi\tau r}{E_m A_m}\left(-\ell^2 + 2\ell_R^2\right) + \alpha_m \Delta T \ell \tag{A16}$$

The extension of the fiber at the minimum load is:

$$\frac{\delta_m^{\min}}{2} + u^{\min} = \int_0^{\ell-\ell_R}\left(\frac{\left(\sigma_f^{BB'}\right)^{\min}}{E_f} + \frac{2\pi\tau r y}{E_f A_f}\right)dy +$$

$$\int_{\ell-\ell_R}^{\ell}\left(\frac{\left(\sigma_f^{BB'}\right)^{\min}}{E_f} + \frac{4\pi\tau r\left(\ell-\ell_R\right)}{E_f A_f} - \frac{2\pi\tau r y}{E_f A_f}\right)dy + \alpha_f \Delta T \ell \tag{A17}$$

which reduces to:

$$\frac{\delta_m^{\min}}{2} + u^{\min} = \frac{\left(\sigma_f^{BB'}\right)^{\min}\ell}{E_f} + \frac{\pi\tau r}{E_f A_f}\left(\ell^2 - 2\ell_R^2\right) + \alpha_f \Delta T \ell \tag{A18}$$

Combining Equations (A10), (A11), (A16), and (A18):

$$\frac{\delta_m^{\min}}{2} = \frac{\tau\eta}{rE_f}\left(\ell^2 - 2\ell_R^2\right) + \Delta T \ell\left(\alpha_f - \alpha_m\right) \tag{A19}$$

By substituting Equation (A8) into (A19):

$$\Delta\delta_m = \frac{4\tau\eta}{rE_f}\ell_R^2 \tag{A20}$$

where $\Delta\delta_m = \delta_m^{\max} - \delta_m^{\min}$. Combining Equations (A14) and (A20) yields the relation between the change in fiber stress along the crack centerline and the change in discrete crack opening displacement from points A to B in Figure A1a:

$$\Delta\delta_m = \frac{r\left(\Delta\sigma_f^{AA'}\right)^2}{4\tau E_f \eta} \tag{A21}$$

The unknown bridging pressure, Δp, and the fiber stress along the matrix crack centerline, $\Delta\sigma_f^{AA'}$, are related through the fiber volume fraction as follows:

$$\Delta p = v_f \Delta\sigma_f^{AA'} \tag{A22}$$

This equation is valid for fibers are closely spaced relative to the crack length. Using Equations (A21) and (A22), the matrix crack opening displacement is related to the unknown bridging pressure:

$$\Delta\delta_m = \lambda \Delta p^2 \tag{A23}$$

where:

$$\lambda = \frac{r}{4\tau v_f^2 E_f \eta} \tag{A24}$$

Reloading: B-A

When reloading back to A, the constant frictional shear stress in ℓ_R reverses direction. Upon reaching A, the shear stress within the entire slip length, ℓ, is in the same direction. The free body diagram in this case is the same as that shown for the original loading case, Figure A1b. Consequently, the discrete crack opening displacement when reloaded to Point A is identical to Equation (A9). Moreover, the change in displacement from Point B to A in Figure A1a is the same as that from Point A to B (Equation (A23)).

APPENDIX B - BOUNDARY CORRECTION FACTOR AND WEIGHT FUNCTION

For two symmetric cracks progressing from a center hole of radius R in an isotropic material, the applied stress boundary correction factor is [16]:

$$F_{app} = F_1 F_2 \tag{B1}$$

where:

$$F_1 = \left(1 + 0.358\frac{R}{a} + 1.425\left(\frac{R}{a}\right)^2 - 1.578\left(\frac{R}{a}\right)^3 + 2.156\left(\frac{R}{a}\right)^4\right)\sqrt{1 - \frac{R}{a}} \tag{B2}$$

and:

$$F_2 = \sqrt{\sec\frac{\pi R}{W}\sec\frac{\pi a}{W}} \tag{B3}$$

For two symmetric cracks emanating from a center notch, F_{app} is obtained by substituting R = 0 into Equations (B2) and (B3).

The weight function, $G(x,a,R,W)$, for two symmetric concentrated forces, P, applied to the cracks surface in a center hole specimen configuration [16]:

$$G(x,a,R,W) = G_{cn} F_h \tag{B4}$$

In this equation, G_{cn} is the weight function for a center notched specimen configuration subjected to a pair of forces, P, on the crack surface and F_h is the correction factor to account for a center hole boundary. The weight function for a center notched specimen is given by [18]:

$$G_{cn} = \left(1 + 0.297\sqrt{1 - \left(\frac{x}{a}\right)^2}\left(1 - \cos\frac{\pi a}{W}\right)\right)F_{III} \tag{B5}$$

where:

$$F_{III} = \sqrt{\frac{1}{W}\tan\frac{\pi a}{W}}\,\frac{\cos\frac{\pi x}{W}}{\sqrt{\cos\left(\frac{\pi x}{W}\right)^2 - \cos\left(\frac{\pi a}{W}\right)^2}} \tag{B6}$$

The correction factor to account for the center hole of radius R is given by [17]:

$$F_h = 1 + A_1\left(\frac{a-x}{a-R}\right) + A_2\left(\frac{a-x}{a-R}\right)^2 \tag{B7}$$

where:

$$A_1 = -0.02\left(\frac{R}{a}\right)^2 + 0.558\left(\frac{R}{a}\right)^4 \tag{B8}$$

$$A_2 = 0.221\left(\frac{R}{a}\right)^2 + 0.046\left(\frac{R}{a}\right)^4 \tag{B9}$$

APPENDIX C - DISCRETE-CONTINUUM RELATIONS AND GOVERNING EQUATIONS

The continuum fracture mechanics analysis and the micromechanics analysis are combined using the following two discrete-continuum relations:

$$\Delta\delta_m = f\left(\Delta\delta_{Comp}\right) \tag{C1}$$

$$\Delta K_m = f\left(\Delta K_{Comp}\right) \tag{C2}$$

Differences among the original fiber bridging models [8-10] arise in defining these two discrete-continuum relations as discussed next.

Crack Opening Displacements

Marshall et al. [8] and McMeeking and Evans [10] assumed that the discrete and the continuum crack opening displacements were equal:

$$\Delta\delta_m = \Delta\delta_{Comp} \tag{C3}$$

McCartney [9] reported that $\Delta\delta_{Comp}$ is actually the change in displacement within the slip region (change in displacement between lines AA' and BB', Figures A1b and A1c) and should be related to $\Delta\delta_m$ as follows:

$$\Delta\delta_m = \Delta\delta_{Comp}\eta \tag{C4}$$

where:

$$\eta = \left(1 + \frac{E_f \nu_f}{E_m \nu_m}\right) \tag{C5}$$

Stress-Intensity Factor

The relation between the matrix and composite stress-intensity factors ranges was established by Marshall et al. [8] using the ratio of the matrix modulus to composite modulus:

$$\Delta K_m = \frac{E_m}{E_L} \Delta K_{Comp} \tag{C6}$$

This equation assumes that the near-tip strains in the composite and in the matrix are compatible. In a different approach, McCartney [9] used an energy balance to relate ΔK_m to ΔK_{Comp} by assuming:

$$\gamma_{Comp} = \nu_m \gamma_m \tag{C7}$$

where $\gamma_{Comp} = K_{Comp}^2 / E_L$ is the fracture surface energy of the composite and $\gamma_m = K_m^2 / E_m$ is the fracture surface energy of the matrix. Rewriting Equation (C7) in terms of stress intensity factor ranges:

$$\Delta K_m = \sqrt{\frac{E_m}{\nu_m E_L}} \Delta K_{Comp} \tag{C8}$$

Finally, it was suggested by McMeeking and Evans [10]:

$$\Delta K_m = \Delta K_{Comp} \tag{C9}$$

In this paper, the discrete-continuum relations derived by Marshall, et al. [8] (Equations (C3) and (C6)), McCartney [9] (Equations (C4) and (C8)) and McMeeking and Evans [10] (Equations (C3) and (C9)) are referred to as the MCE, MC, and ME relations, respectively.

Governing Equations

The crack opening displacements from the micromechanics analysis, Equation (2), and from the continuum analysis, Equation (6), are combined using discrete-continuum relations, Equation (C1) to yield a single nonlinear integral equation in terms of the unknown bridging pressure, Δp, and the unknown frictional shear stress τ. Using Equation (C3), the MCE [8] or ME [10] relation:

$$\Delta p^2 = \frac{2}{\lambda E'} \int_x^a \left(\Delta S \sqrt{\pi a} F_{app} - 2 \int_{a_o}^a \Delta p G(x,a,R,W) dx \right) G(x,\tilde{a},R,W) d\tilde{a} \qquad \text{(C10)}$$

Using the MC relation [9], namely, Equation (C4):

$$\Delta p^2 = \frac{2}{\eta \lambda E'} \int_x^a \left(\Delta S \sqrt{\pi a} F_{app} - 2 \int_{a_o}^a \Delta p G(x,a,R,W) dx \right) G(x,\tilde{a},R,W) d\tilde{a} \qquad \text{(C11)}$$

Assuming a value for τ, the bridging pressure, Δp, is solved using a Newton-Raphson iterative procedure and a Simpson type algorithm for numerical integration. Once the bridging pressure is known, the matrix stress intensity factor range, ΔK_m, can be obtained using Equations (8) and (C2). Using the MCE relation [10], namely, Equation (C6):

$$\Delta K_m = \frac{E_m}{E_L} \left(\Delta S \sqrt{\pi a} F_{app} - 2 \int_{a_o}^a \Delta p G(x,a,R,W) dx \right) \qquad \text{(C12)}$$

Using the MC relation [9], namely, Equation (C8):

$$\Delta K_m = \sqrt{\frac{E_m}{\nu_m E_L}} \left(\Delta S \sqrt{\pi a} F_{app} - 2 \int_{a_o}^a \Delta p G(x,a,R,W) dx \right) \qquad \text{(C13)}$$

Using the ME relation [10], namely, Equation (C9):

$$\Delta K_m = \Delta S \sqrt{\pi a} F_{app} - 2 \int_{a_o}^a \Delta p G(x,a,R,W) dx \qquad \text{(C14)}$$

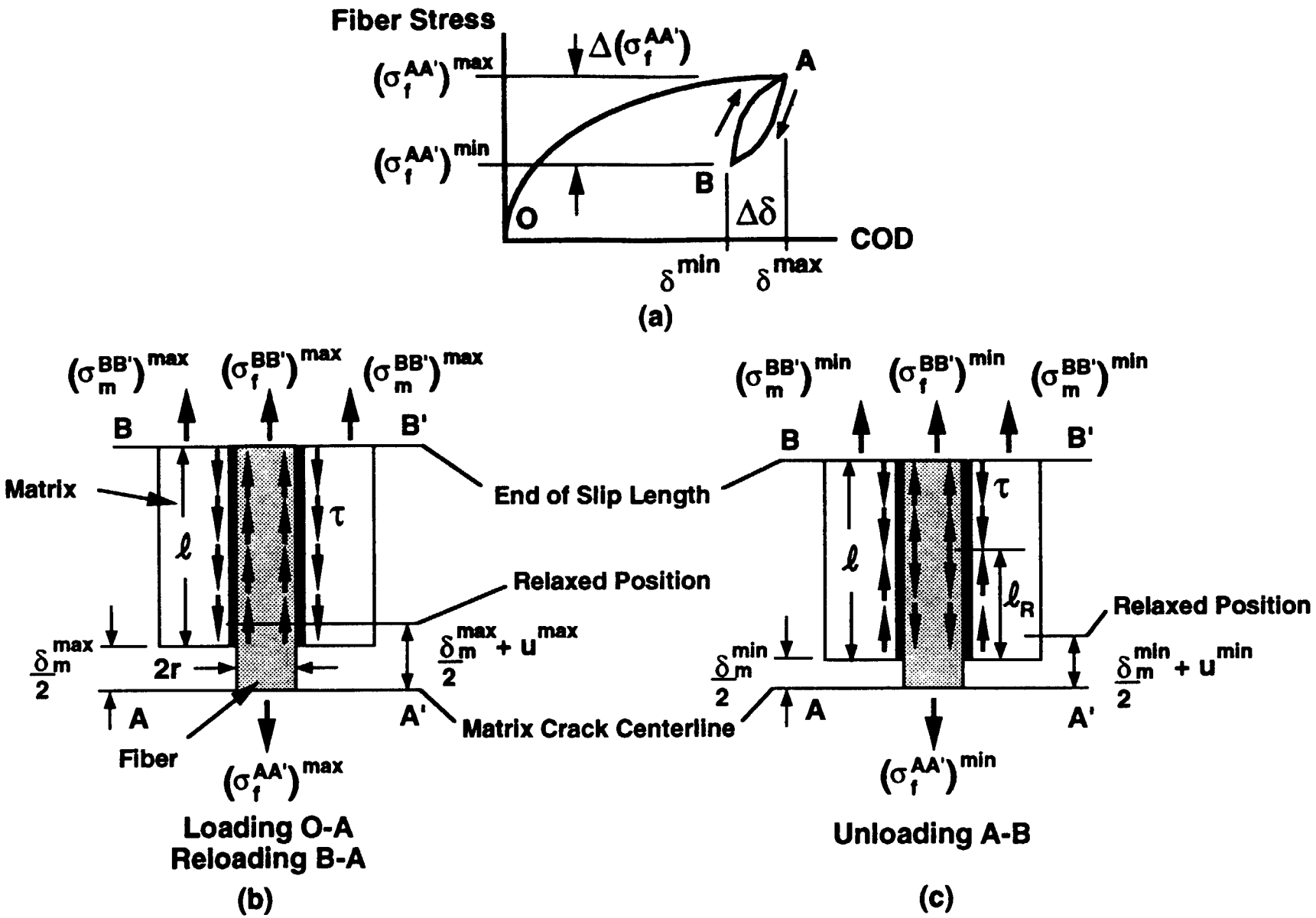

Figure A1. Micromechanics of fiber bridging: (a) Fiber stress as a function of crack opening displacement; (b) Free body diagram of fiber in wake of crack at maximum applied load; and (c) Free body diagram of fiber in wake of crack at minimum applied load.

REPORT DOCUMENTATION PAGE

Form Approved
OMB No. 0704-0188

1. AGENCY USE ONLY (Leave blank)	2. REPORT DATE	3. REPORT TYPE AND DATES COVERED
	February 1994	Technical Memorandum

4. TITLE AND SUBTITLE

Implementation of Thermal Residual Stresses in the Analysis of Fiber Bridged Matrix Crack Growth in Titanium Matrix Composites

5. FUNDING NUMBERS

WU 505-63-50-04

6. AUTHOR(S)

John G. Bakuckas, Jr. and W. Steven Johnson

7. PERFORMING ORGANIZATION NAME(S) AND ADDRESS(ES)

NASA Langley Research Center
Hampton, VA 23681-0001

8. PERFORMING ORGANIZATION REPORT NUMBER

9. SPONSORING/MONITORING AGENCY NAME(S) AND ADDRESS(ES)

National Aeronautics and Space Administration
Washington, DC 20546-0001

10. SPONSORING/MONITORING AGENCY REPORT NUMBER

NASA TM 109082

11. SUPPLEMENTARY NOTES

Bakuckas, Jr.: Galaxy Scientific Corporation, Pleasantville, NJ; Johnson: Langley Research Center, Hampton, VA

12a. DISTRIBUTION/AVAILABILITY STATEMENT

Unclassified - Unlimited

Subject Category 24

12b. DISTRIBUTION CODE

13. ABSTRACT *(Maximum 200 words)*

In this research, thermal residual stresses were incorporated in an analysis of fiber-bridged matrix cracks in unidirectional and cross-ply titanium matrix composites (TMC) containing center holes or center notches. Two TMC were investigated, namely, SCS-6/Timetal-21S laminates. Experimentally, matrix crack initiation and growth were monitored during tension-tension fatigue tests conducted at room temperature and at an elevated temperature of 200°C. Analytically, thermal residual stresses were included in a fiber bridging (FB) model. The local R-ratio and stress-intensity factor in the matrix due to thermal and mechanical loadings were calculated and used to evaluate the matrix crack growth behavior in the two materials studied. The frictional shear stress term, τ, assumed in this model was used as a curve-fitting parameter to matrix crack growth data. The scatter band in the values of τ used to fit the matrix crack growth data was significantly reduced when thermal residual stresses were included in the fiber bridging analysis. For a given material system, lay-up and temperature, a single value of τ was sufficient to analyze the crack growth data. It was revealed in this study that thermal residual stresses are an important factor overlooked in the original FB models.

14. SUBJECT TERMS

Fiber-matrix debonding; Stress intensity factor; Crack growth; Metal matrix composites micromechanics; Fracture mechanics

15. NUMBER OF PAGES

43

16. PRICE CODE

A03

17. SECURITY CLASSIFICATION OF REPORT	18. SECURITY CLASSIFICATION OF THIS PAGE	19. SECURITY CLASSIFICATION OF ABSTRACT	20. LIMITATION OF ABSTRACT
Unclassified	Unclassified		